

1

# 1 Coastal and regional marine heatwaves and cold-spells in 2 the Northeast Atlantic

3

4 Amélie Simon<sup>1\*</sup>, Coline Poppeschi<sup>2</sup>, Sandra Plecha<sup>1</sup>,  
5 Guillaume Charria<sup>2</sup>, Ana Russo<sup>1</sup>

6

7 <sup>1</sup> Universidade de Lisboa, Faculdade de Ciências, Instituto Dom Luiz (IDL), 1749-016, Lisboa, Portugal

8 <sup>2</sup> Ifremer, Univ. Brest, CNRS, IRD, Laboratory for Ocean Physics and Satellite remote sensing (LOPS), IUEM,  
9 29280 Brest, France

10

11 \*corresponding author: Dr. Amélie Simon; ajsimon@fc.ul.pt

12

13

## 14 Abstract

15

16 The latest IPCC report describes an increase in the number and intensity of marine heatwaves  
17 (MHWs) and a decrease in marine cold-spells (MCSs) in the global ocean. However, these  
18 reported changes are not uniform on a regional to local basis and it remains unknown if  
19 coastal areas follow the open ocean trends. Surface ocean temperature measurements  
20 collected by satellites (from 1982-2022) and 13 coastal buoys (from 1990-2022) are analyzed  
21 in the northeast Atlantic and three subregions: English Channel, Bay of Brest and Bay of  
22 Biscay. The activity metric, combining the number of events, intensity, duration and spatial  
23 extent, is used to evaluate the magnitude of these extreme events. The results from *in situ* and  
24 satellite datasets for each of the studied regions are quite in agreement, although the satellite  
25 dataset underestimates the amplitude of activity for both MHWs and MCS. This supports the  
26 applicability of the method to both *in situ* and satellite data, albeit with caution on the  
27 amplitude of these events. Also, this localized study in European coastal northeast Atlantic  
28 water highlights that similar changes are being seen in coastal and open oceans regarding  
29 extreme events of temperature, with MHWs being more frequent, longer, and extending over  
30 larger areas, while the opposite is seen for MCSs. These trends can be explained by changes  
31 in both the mean and variance of sea-surface temperature. In addition, the pace of evolution  
32 and dynamics of marine extreme events differs among the subregions. Among the three  
33 studied subregions, the English Channel is the region experiencing the strongest increase in  
34 summer MHWs activity over the last four decades. Summer MHWs were very active in the  
35 English Channel in 2022 due to long events, in the Bay of Biscay in 2018 due to intense  
36 events and in the Bay of Brest in 2017 due to a high occurrence of events. Winter MCSs were  
37 the largest in 1987 and 1986 due to long and intense events in the English Channel. Finally,  
38 our findings suggest that at an interannual time scale, the positive North Atlantic Oscillation  
39 favors the generation of strong summer MHWs in the northeast Atlantic, while dominant low-  
40 pressure conditions over northern Europe and a high off the Iberian Peninsula in winter  
41 dominates for MCSs. A preliminary analysis of air-sea heat fluxes suggests that, in this  
42 region, reduced cloud coverage is a key parameter for the generation of summer MHWs while  
43 strong winds and increased cloud coverage is important for the generation of winter MCSs.

44

45

46

47

48

49

50

51  
5253 **Keywords**

54

55 Extreme events, Sea Surface Temperature, Long-term *in situ* observations, Satellite data,  
56 Marine heatwaves, Marine cold-spells, Bay of Biscay, English Channel, North Atlantic  
57 Oscillation

58

59

60

61

62 **1. Introduction**

63

64 Heatwaves and cold-spells are extreme events in which there is a strong anomaly in  
65 temperature for a certain period which can occur at a regional spatial scale. This type of  
66 phenomenon can occur both in the atmosphere and in the ocean, with remarkable  
67 consequences both for terrestrial and marine ecosystems (Ruthrof et al., 2018). In the case of  
68 marine events (hereafter referred to as marine heatwaves (MHWs) or marine cold-spells  
69 (MCSs)), severe large-scale biodiversity losses may occur such as species extinction, habitat  
70 destruction and abrupt changes in the geographical distribution and structure of communities,  
71 as well as the nutrient cycle (Frölicher and Laufkötter, 2018; Ruthrof et al., 2018; Smale et al.,  
72 2019). Additionally, a decrease in the density of marine algae forests and coral bleaching  
73 (Wernberg et al., 2016; Smale et al., 2019) have also been reported.74 The frequency, duration and intensity of these extreme phenomena affecting ocean  
75 systems have been increasing in recent decades (Lima and Wetthey, 2012; Oliver et al., 2018;  
76 Frölicher et al., 2018; Plecha and Soares, 2020; Simon et al., 2022 and many others). As a  
77 result of global and regional warming heavily influenced by anthropogenic factors, the  
78 intensity and annual number of MHWs will continue to accelerate globally (Oliver et al.,  
79 2019; Plecha et al., 2021). Conversely, as oceans warm, MCSs are diminishing (Schlegel et  
80 al., 2021; Simon et al., 2022) and are expected to continue to decline in the future (Yao et al.,  
81 2022). However, these changes are not uniform regionally and it remains unknown if coastal  
82 areas follow the open-ocean trends.83 This paper focuses on the coastal and regional northeast Atlantic and three subregions  
84 (English Channel, Bay of Brest and Bay of Biscay) as these zones are important for socio-  
85 economic activities (e.g. fishery; Guo et al., 2022) and have contrasted dynamical  
86 environments. Plecha et al. (2021) studied MHWs annual features in the whole north Atlantic  
87 using low-resolution satellite data at  $1^\circ \times 1^\circ$  over the period 1971-2000. They show that in the  
88 Bay of Biscay, the mean frequency is about 12 events per year and is characterized by  $\sim 12$   
89 days of mean duration and  $0.4^\circ\text{C}$  of mean intensity. Marin et al. (2021) did a global analysis  
90 of MHWs in coastal areas over the period 1992–2016 based on a multi-satellite product at a  
91 resolution from  $0.25^\circ \times 0.25^\circ$  to  $0.05^\circ \times 0.05^\circ$ . They found that in the Bay of Biscay and English  
92 Channel from 1992–2016, MHWs occurred on average 3 times per year lasting about 20 days  
93 with a mean intensity of  $1.5^\circ\text{C}$ . Here we focus on these regions at the seasonal time-scale,  
94 such as summer MHWs and winter MCSs using a satellite product at  $0.25^\circ \times 0.25^\circ$ .

95

96 Long-term ocean warming is an important driver of the increase of MHWs (Frölicher  
97 et al., 2018) and the diminishing of MCSs (Schlegel et al., 2021; Wang et al., 2022) but does

98 not explain shorter variabilities of these events, or their interannual variability. These marine  
99 extreme events are also driven by other local and remote processes acting across a large range  
100 of spatial and temporal scales (Holbrook et al., 2019; Schlegel et al., 2021). Modes of  
101 atmospheric circulation variability can induce anomalous sea surface temperature (SST)  
102 through modification of air-sea heat fluxes and/or displacement due to ocean current  
103 advection (Deser et al., 2010) which for extreme cases, can lead to MHWs or MCS.

104 Interannual summer atmospheric variability in the north Atlantic-European sector has  
105 been shown to be predominantly led by the summer north Atlantic Oscillation (SNAO)  
106 pattern. The SNAO is identified as strong high-pressure anomalies dominating northern  
107 Europe and weaker low-pressure over Greenland and the Iberian Peninsula which explains  
108 about 20% of the variance using sea-level pressure (Hurrell et al., 2003). The SNAO is  
109 recognized as a more northerly location and smaller spatial scale than the winter NAO pattern.  
110 During the positive phase of the SNAO, northern Europe experiences drier, warmer and  
111 reduced cloudiness conditions, and the Bay of Biscay, the English Channel, and the north and  
112 Baltic Seas undergo warmer SST (Folland et al., 2009). The East Atlantic (EA) pattern is also  
113 identified as a dominant mode of north Atlantic atmospheric variability (Barnston and  
114 Livezey, 1987), which is particularly important for the northwest Iberian Peninsula climate in  
115 all seasons (Lorenzo et al., 2008). It is a north–south dipole that spans the entire north Atlantic  
116 Ocean, with centers southeastward to the NAO pattern (winter and summer).

117 Although there is strong evidence of the influence of large-scale features, no  
118 consensus exists on atmospheric patterns associated with summer MHWs in the Bay of  
119 Biscay and the English Channel. On one side, Holbrook et al. (2019) identify the Bay of  
120 Biscay as a region for which there is a significant increase in annual MHWs days during a  
121 positive phase of the NAO, based on a linearly detrended SST with satellite data and NAO  
122 index. On the other side, Izquierdo et al. (2022a) suggest, based on the analysis of two *in situ*  
123 buoys in the coastal south of the Bay of Biscay, that the incidence, duration, and intensity of  
124 spring-summer MHWs is higher during the positive phase of the EA. However, for each of  
125 these two studies, only one climate index out of the numerous modes of summer atmospheric  
126 variability in the north Atlantic-Europe sector was considered.

127 MCSs have also been reported to occur as a response to atmospheric forcing through  
128 anomalous winds and air-sea heat fluxes, especially in coastal regions where cold air  
129 outbreaks over shallow water can cause rapid chilling of water (Crisp, 1964; Schlegel et al.,  
130 2021). But to the best of our knowledge, no study has been published focusing on the  
131 connection between MCSs and atmospheric circulation in the Bay of Biscay and the English  
132 Channel.

133  
134 At a more regional scale, Guinaldo et al. (2023) linked the 2022 MHW off France to  
135 above-average solar radiation, below-average cloud coverage and negative wind speed  
136 anomalies showing also the importance of hydrodynamic conditions such as the tide that  
137 allows turbulent vertical mixing. This explains why the Mediterranean sea with weak tidal  
138 ranges presents a more pronounced response to MHWs (Darmaraki et al., 2019; Simon et al.,  
139 2022). Other studies have been carried out in terms of processes and detection of MHWs in  
140 the Bay of Biscay but only along the Spanish Cantabrian coast. Namely, Izquierdo et al.  
141 (2022b), found a steady increase in SST from 1998 to 2019, which was reflected in MHWs  
142 occurrence and consequent match-up to report population shifts in coastal macroalgae. In a  
143 second study, Izquierdo et al. (2022a) compared MHWs with satellite data and found a 6-fold  
144 increase in their incidences in the last four decades with half of this increase related to climate  
145 change.

146 Several studies focus on the impact of MHWs or MCSs on biological systems,  
147 covering the areas of the Bay of Biscay, the English Channel or the Spanish Cantabrian coast,

148 reaching as far back as the 60s of the 20th century. These studies analyzed the atmospheric  
149 cold-spells of the winter of 1962-1963 on the English coast and the impact on marine animal  
150 mortality such as *Pecten Maximus* (Crisp, 1964) or migration of species such as flounder  
151 (Sims et al., 2004). In the English Channel, Gomez and Souissi (2008) made the link between  
152 the MCS of 2005 and the absence of the spring bloom of *Phaeocystis*. A delay in the initiation  
153 of the phytoplankton bloom caused by the presence of MCS at the end of winter in the Bay of  
154 Brest and in the Bay of Vilaine (in the northern part of the Bay of Biscay) is observed by  
155 Poppeschi et al. (2022). The impact of MHWs on biology is even more studied than the cold  
156 counterpart. Gomez and Souissi (2008) show the link between the heatwave of 2003 in the  
157 English Channel and the abundance of dinoflagellates. Joint and Smale (2017) demonstrate a  
158 link between MHWs and microbial activity assemblage in the English Channel which controls  
159 biogeochemical cycles in the ocean. The MHW of 2018 in the English Channel is present in  
160 the literature for its mortality mass impact on mussels (Seuront et al., 2019), its link to fucoids  
161 (Mieszkowska et al., 2020) or harmful phytoplankton blooms (Brown et al., 2022).  
162 Predictions at the atmospheric scale point to an increase in the future of heatwaves in the Bay  
163 of Biscay (Chust et al., 2011) and a decrease in marine fauna (Wethey and Woodin, 2022).

164

165 In this context, we aim to describe and explain the evolutions of the MHWs over  
166 summer and MCSs over winter activity in the northeast Atlantic and to investigate the  
167 regional variability in three subregions: the English Channel, the Bay of Brest and the Bay of  
168 Biscay. The analysis will rely on both *in situ* and satellite data to address MHWs and MCSs  
169 activity, aiming to evaluate the impact of such events in coastal regions and in the open ocean.  
170 This approach will allow us to evaluate the potential use of *in situ* measurements to detect,  
171 characterize and understand such extreme events. In the last section of this paper, we focus on  
172 the influence of the interannual atmospheric mode of variability involved in the occurrence of  
173 MHWs and MCSs in the northeast Atlantic by finding the atmospheric circulation occurring  
174 in phase with most of the strongest events.

175

176

## 177 2. Material and methods

178

### 179 2.1 Satellite and reanalysis data

180

181 The global SST data used in this study results from a combination of different  
182 observational platforms, including satellites, ships, buoys and Argo floats, provided by the  
183 National Oceanic and Atmospheric Administration (hereafter OISST; Reynolds et al., 2007;  
184 Huang et al., 2020). The satellite products have a daily temporal coverage for the 1982-2022  
185 period and are interpolated to a regular global grid of  $1/4^\circ$  spatial resolution. Monthly  
186 geopotential height at 500 hPa (Z500), surface net short-wave radiation flux, surface net long-  
187 wave radiation flux, surface sensible heat flux and latent radiation heat flux data were  
188 obtained from the European Center for Medium-Range Weather Forecasts (ECMWF)  
189 reanalysis data ERA5 at a spatial resolution of  $0.25^\circ \times 0.25^\circ$  (Hersbach et al., 2019).

190

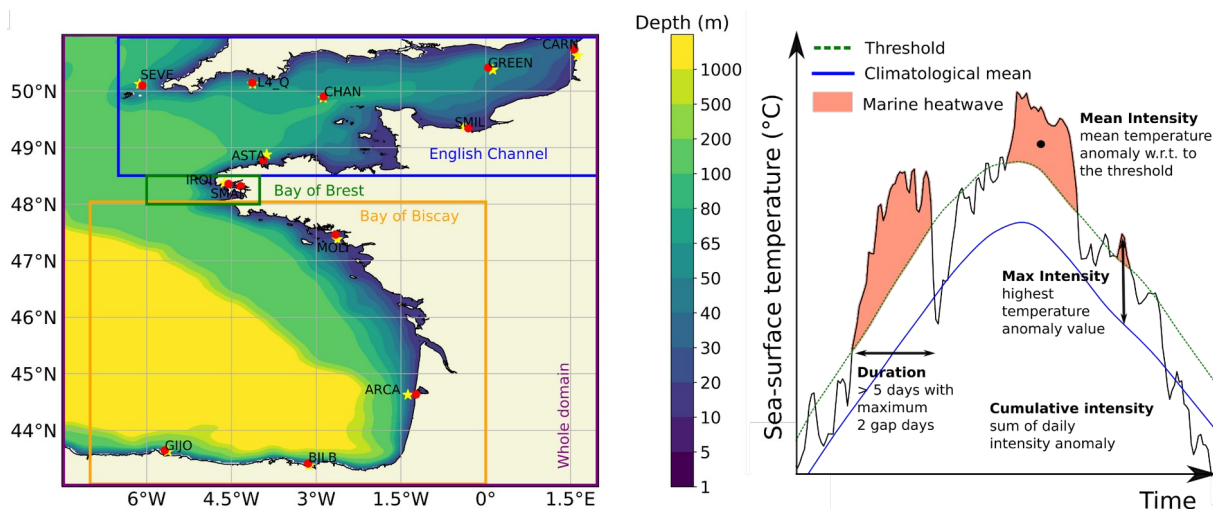
191

### 192 2.2 Buoy data

193

194 The *in situ* SST data are from autonomous coastal buoys that take continuous high-  
195 frequency measurements from 10 minutes to 1 hour (Figure 1, left panel). These buoys are  
196 from different European organizations, detailed below and in Table S1, covering the coastal  
197 areas of the English Channel, the Bay of Brest and the Bay of Biscay.

198 The National Observation Infrastructure network (COAST-HF, [www.coast-hf.fr](http://www.coast-hf.fr))  
 199 operates 14 buoys taking measurements of several physical and biogeochemical all around  
 200 French coasts. Among them, 7 buoys are used here and are located in the English Channel -  
 201 CARNot (<https://doi.org/10.17882/39754>), SMILe (<https://doi.org/10.17882/53689>) and  
 202 ASTAn; in the Bay of Brest - IROise (<https://doi.org/10.17882/74004>) and SMARt  
 203 (<https://doi.org/10.17882/86020>) and in the Bay of Biscay - MOLIt  
 204 (<https://doi.org/10.17882/46529>) and ARCAchon. The Met Office ([www.metoffice.gov.uk](http://www.metoffice.gov.uk))  
 205 manages several buoys and also at offshore sites. The buoys used here are located in the  
 206 English Channel, on the South coast of England, SEVEN Stones; CHANnel and GREENwich.  
 207 The western Channel Observatory (WCO, [www.westernchannelobservatory.org.uk](http://www.westernchannelobservatory.org.uk)), situated  
 208 within the western English Channel operates two oceanographic moorings. The station L4\_Q  
 209 located near the city of Plymouth, approximately 7 km offshore is used here. Puertos del  
 210 Estado ([www.puertos.es](http://www.puertos.es)) operated two buoys along the Spanish coast: BILBao and GIJOn  
 211 located in the Cantabrian Sea, both of them are used here.  
 212



213 Figure 1: (Left) Map of the study area including the whole domain/northeast Atlantic (purple  
 214 box) as well as the three subregions which are the English Channel (blue box), the Bay of  
 215 Brest (green box) and the Bay of Biscay (orange box). The buoys are represented by red dots  
 216 and the closest satellite points are represented by yellow stars. (Right) Schematic of MHW  
 217 detection and properties as defined by Hobday et al. (2016).  
 218

219

220

### 221 2.3 Detection of MHWs and MCS

222

223 To detect marine temperature extreme anomalies, we use the definition of Hobday et  
 224 al. (2016). First, a climatology over 40 years, from 1982 to 2022, is calculated from the  
 225 satellite product. Then, we apply the 90<sup>th</sup> percentile on summers (JJAS) for MHW and the 10<sup>th</sup>  
 226 on winters (DJFM) for MCS. Finally, a MHW (MCS) is detected if values are above (below)  
 227 the threshold for at least 5 days. For *in situ* data, the same detection method is applied  
 228 considering the climatology calculated from the satellite product. Only seasons (summer or  
 229 winter) with more than 80% of available data are analyzed.

230 To characterize MHW and MCS, we analyze parameters such as the number of events,  
 231 the duration, the spatial extent and the cumulative intensity, defined as in Hobday et al. (2016)  
 232 (Figure 1, right panel). We also explore an integrated indicator of these different parameters  
 233 characterizing the marine temperature extreme events (MHWs and MCS), called activity and  
 234 defined by Simon et al. (2022). This indicator estimates for each grid point the cumulative

235 combination of the mean intensity, the duration and the affected area of each extreme event  
 236 within a selective time range (for example JJAS). This activity index accounts explicitly for  
 237 the area, as in most SST products a grid cell area differs from one latitude to another and  
 238 marine thermal events can expand over large areas. The activity is calculated for each grid  
 239 point. It sums the product of the mean intensity, duration within the selected time range, and  
 240 area of each detected event occurring within the selected time range. The activity is written as  
 241 follows:

$$242 \text{ Activity} = \sum_{EE \in \text{Time Range}} \text{mean intensity}_{EE} \cdot \text{duration}_{EE \cap \text{Time Range}} \cdot \text{area}_{EE}$$

243  
 244 Where  $EE \in \text{time range}$ , denotes the extreme event (EE) that occurs within the selected time  
 245 range; the mean intensity of EE (in °C) is the mean temperature anomaly with respect to the  
 246 threshold of the event; duration  $EE \cap \text{time range}$  (in days) is the duration of the event that  
 247 remains within the considered time range, and  $\text{area}_{EE}$  (in km<sup>2</sup>) is the area affected by the  
 248 discrete event within a predefined domain. Time series involving the activity metric for a  
 249 domain are calculated as the mean of every grid cell considered. The activity for each station  
 250 is computed in °C.days without considering the area influenced by the events as it can not be  
 251 estimated from single localized stations.

252 This method of detection and characterization of marine thermal extreme events is  
 253 performed over the whole domain of this study, referred to as the northeast Atlantic (8° W to  
 254 2° E - 43° N to 51° N) and at each station where *in situ* observations are available. As  
 255 illustrated in Figure 1, three different subregions will be analyzed in detail, namely (i) the  
 256 English Channel (6.5° W to 2° E - 48.5° N to 51° N), (ii) the Bay of Brest (6° W to 4° W -  
 257 48° N to 48.5° N) and (iii) the Bay of Biscay (7° W to 0° W - 43° N to 48° N). This will allow  
 258 us to explore these regions separately and highlight regional patterns. Those three subregions  
 259 can be associated with three contrasted hydrodynamical regimes: macrotidal (English  
 260 Channel), semi-enclosed bay (Bay of Brest), mesotidal (Bay of Biscay; Charria et al., 2013).

261

## 262 3. Results

263

### 264 3.1 Evolution of marine heatwave activity

265

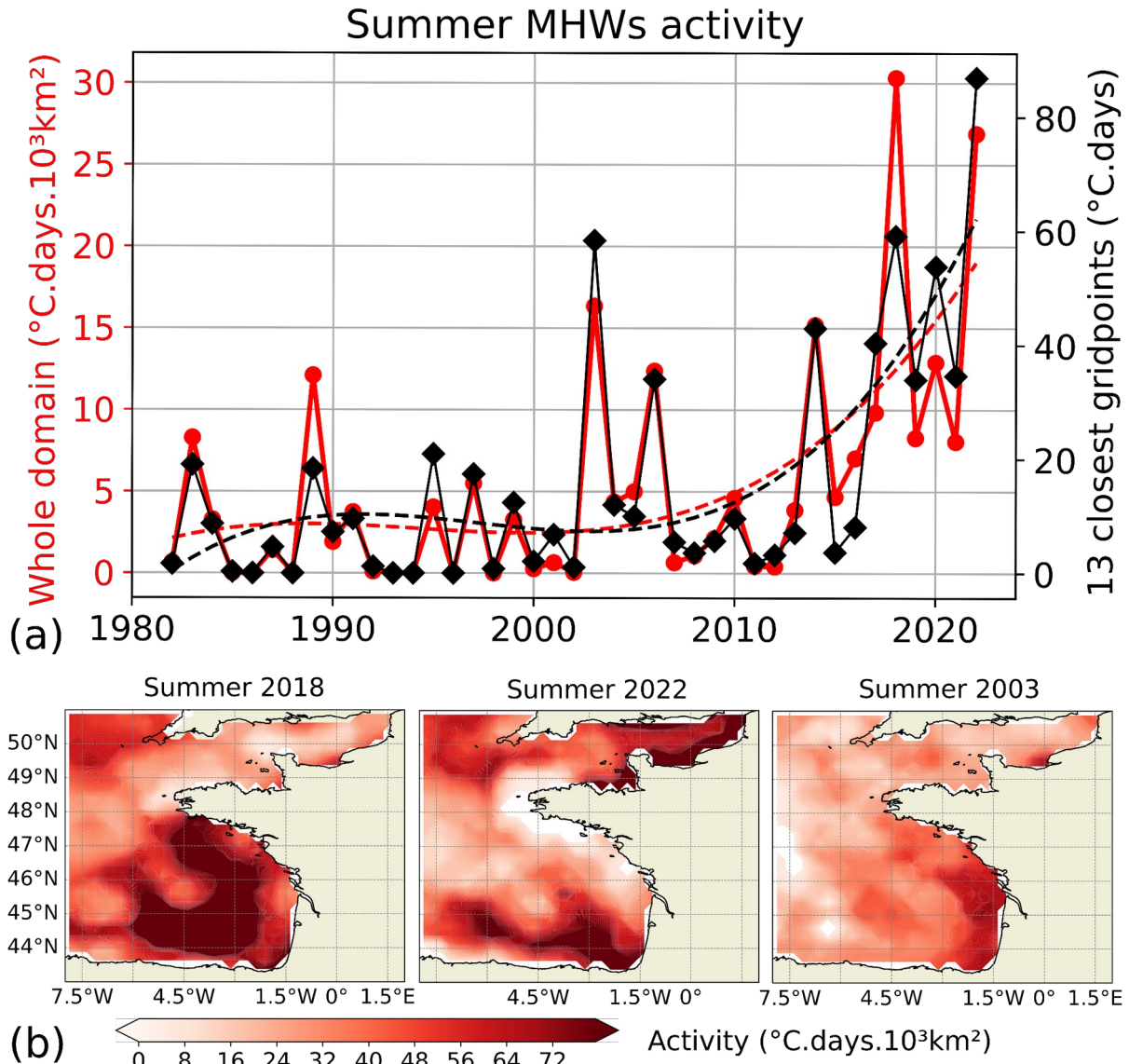
#### 266 3.1.1. An integrated regional view

267

268 MHWs were detected over the northeast Atlantic. The activity index (Figure 2a)  
 269 highlights two main periods in the MHWs dynamics. Before 2003, MHWs activity remained  
 270 moderate to weak with activity generally lower than 5 °C.days.10<sup>3</sup> km<sup>2</sup> corresponding to 1.2  
 271 mean occurrences per summer with a mean duration limited to 8 days (Figure 3). Only the  
 272 summer of 1989 displayed strong MHWs activity (exceeding 10 °C.days.10<sup>3</sup> km<sup>2</sup>) before  
 273 2000. From 2003 onward, the activity increased over 30 °C.days.10<sup>3</sup> km<sup>2</sup> for summers 2018  
 274 and 2022 associated with more than 2.5 mean occurrences lasting around 20 days. The mean  
 275 intensity remains quasi-steady during the whole period. The interannual variability and trend  
 276 of the summer MHWs activity for the whole domain is similar to the one obtained for the  
 277 average activity of the 13 grid cells closest to the buoy locations (black line of Figure 2),  
 278 suggesting that at first order of magnitude, coastal and open ocean follow the same evolution.

279

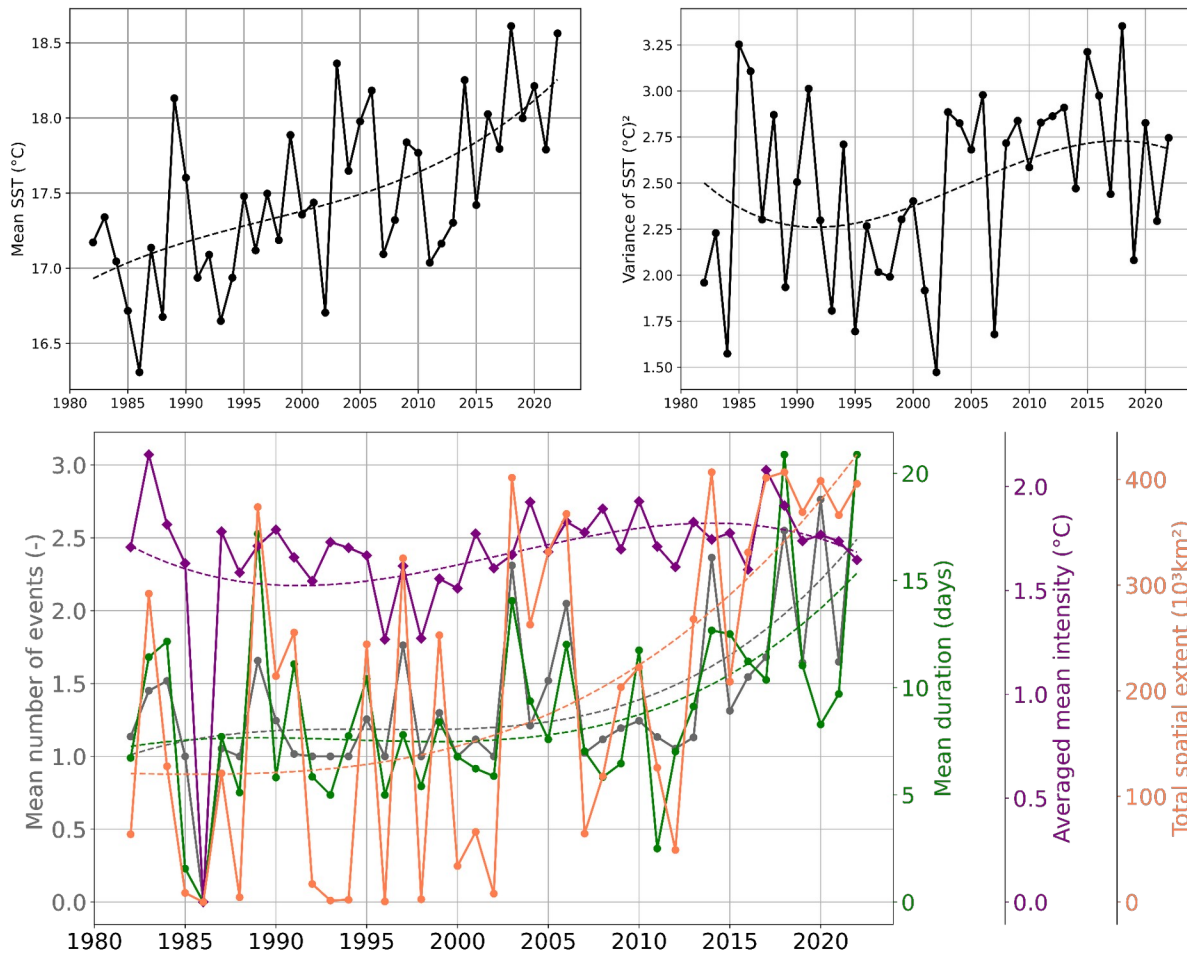
280



281  
 282 Figure 2: (a) Times series of summer (JJAS) MHWs mean activity in the northeast Atlantic  
 283 from the satellite product (red curves with circle marks) and for the average of the 13 grid  
 284 cells closest to the buoys from the satellite product (black curves with diamond marks). Dash  
 285 lines represent the regression of a third-order polynomial of the solid line with the same color.  
 286 (b) Summer (JJAS) activity (first row; in  $^{\circ}\text{C.days}\cdot 10^3\text{ km}^2$ ) for the top 3 summers in terms of  
 287 activity in the northeast Atlantic (from left to right).

288  
 289 The three most active summers are 2018, 2022 and 2003 (Figure 2a). During 2018  
 290 (Figure 2b), maximum activity is located in the Bay of Biscay over the outer continental shelf  
 291 and the continental slope from the southern part of the Biscay. These events are also  
 292 extending to the north to southern of Brittany and is limited by the Ushant tidal front (Le  
 293 Boyer et al., 2009; Müller et al., 2010). Regions of minimum activity during 2018 are west of  
 294 French Brittany in the Ushant front region where tides are efficiently mixing the water  
 295 column. Similarly, the activity remains weak in the English Channel, as it is a macrotidal  
 296 region. In terms of duration, longer events are observed in the southern part of the Bay of  
 297 Biscay exceeding 30 days (Figure S1). The 2022 summer is the second most active year for  
 298 the whole domain, with over  $25\text{ }^{\circ}\text{C.days}\cdot 10^3\text{ km}^2$ , and also the strongest in terms of marine  
 299 activity over coastal regions as shown by the maximum value of the average activity near the  
 300 13 buoys considered (Figure 2a). Spatially, the English Channel and the north of Spain record

301 the strongest MHWs activity while the French Brittany coast has no occurrence over this year  
 302 (Figure 2b). In the English Channel, the mean duration of the summer 2022 events was  
 303 around 35 days (Figure S2) with localized events lasting more than 50 days (Figure S1). In  
 304 northern Spain, the duration of the events was around 20 days, however, they occurred very  
 305 frequently over the summer with strong mean MHWs intensities of around 2 °C (Figure S1).  
 306 In 2003 (Figure 2c), the MHWs activity spatial distribution was different than in 2018 and  
 307 2022. The activity is larger over the inner continental shelf along western French coasts in the  
 308 Bay of Biscay. This region is under the influence of significant river plumes along this coast  
 309 (Adour, Gironde and Loire rivers). During this year, river discharge could have induced  
 310 stratification (inducing faster warming of the surface mixed layer in regions of freshwater  
 311 influence; Oh et al., 2023) and warmer waters from rivers suggest that observed MHWs were  
 312 sustained by an atmospheric event more centered over lands. During this summer, the number  
 313 of events is larger in the western English Channel but shorter and less intense than in the Bay  
 314 of Biscay. These top three active summers highlight the interannual spatial variability of  
 315 MHWs activity. The detailed mean features (number of events, duration and mean intensity)  
 316 of summer MHWs over the period 1982-2022 in the northeast Atlantic, English Channel, Bay  
 317 of Brest and Bay of Biscay are documented in Table S2.  
 318



319 Figure 3: Time series of the mean (upper-left) and variance (upper-right) of SST (black curve)  
 320 of summers (JJAS) over the northeast Atlantic for the period 1982-2022. The SST variance is  
 321 calculated for each year over the respective domain and measures the spread of the spatial  
 322 distribution. (Bottom) Mean properties of summer (JJAS) MHWs in the northeast Atlantic.  
 323 The mean number of events (grey curve with circle marks) is the number of events within the  
 324 summer averaged over the domain (without considering cells with zero event). Mean duration  
 325



326 (green curve with circle marks) is the average duration of every event within the summer and  
327 domain. Averaged mean intensity (purple curve with diamond marks) is the average of the  
328 mean intensity of every event within the period and domain. Total spatial extent (orange curve  
329 with circle marks) is the sum of each grid cell area where one or more events occur. If more  
330 than one MHWs occurs on the same cell, only one grid cell area is taken into account. Dash  
331 lines represent the regression of a third-order polynomial of the solid line with the same color.  
332

333 The mean SST has been increasing over the 40 years with an approximately linear  
334 trend, showing a mean warming of nearly 1.5 °C for the whole domain since 1982 (Figure 3).  
335 Regionally, it is observed that the increase in the mean SST is almost yearly constant for the  
336 Bay of Biscay region, and quadratic for the English Channel and Bay of Brest, where a  
337 plateau is observed around 1995-2010 (Figure S2).

338 The SST variance is calculated for each year over the respective domain and measures  
339 the spread of the spatial distribution. Over the northeast Atlantic, during 1985-2002 and the 5  
340 most recent years are characterized by a decline in the SST variance, while around 1992-2017  
341 an increase in the SST variance is observed. This interannual trend is similar to the ones  
342 observed for the events' intensity, with the exception of the English Channel, showing a direct  
343 relationship between the SST variance and the mean intensity of the MHWs events. In the  
344 English Channel, Bay of Brest and Bay of Biscay, the mean SST is warming and the variance  
345 is increasing. This estimation suggests that they both contribute to the changes in the  
346 respective MHWs activity (Figure S2).

347 Contributing to this recent increase in the northeast Atlantic is primarily the sharp  
348 trend of the events' spatial extent ( $\sim 180$  to  $400$  °C.days. $10^3$  km<sup>2</sup>), followed by the rise of the  
349 number of events (1.2 to 2.5) and also their duration (7 to 15 days; Figure 3). One should note  
350 that, for the same number of events, the events' spatial extent can differ depending on their  
351 spatial repartition, as in the events' spatial extent only one grid cell area is taken into account  
352 when more than one event occurs on the same grid. Furthermore, over the most recent years  
353 the mean number of events, their mean duration and total spatial extent reached the maximum  
354 recorded values. Since 2017, the total spatial extent over the northeast Atlantic has recorded  
355 consecutive high values, exceeding  $360 \times 10^3$  km<sup>2</sup>. The summers of 2018, 2020 and 2022  
356 recorded on average more than 2.5 events for almost all subregions, with events lasting on  
357 average more than 20 days in 2018 (Bay of Biscay) and 2022 (English Channel; Figure S2).  
358 Among the three studied subregions, the English Channel is the region experiencing the  
359 strongest increase in summer MHWs activity over the last four decades (see trend in Figure  
360 S3). The longest mean duration is seen in the English Channel (35 days in summer 2022), the  
361 highest mean number of events occurred in the Bay of Brest (2.7 in summer 2020) and the  
362 highest mean intensity is present in the Bay of Biscay (2.2 °C in 2017; Figure S2).  
363

### 364 3.1.2. Coastal MHWs activity

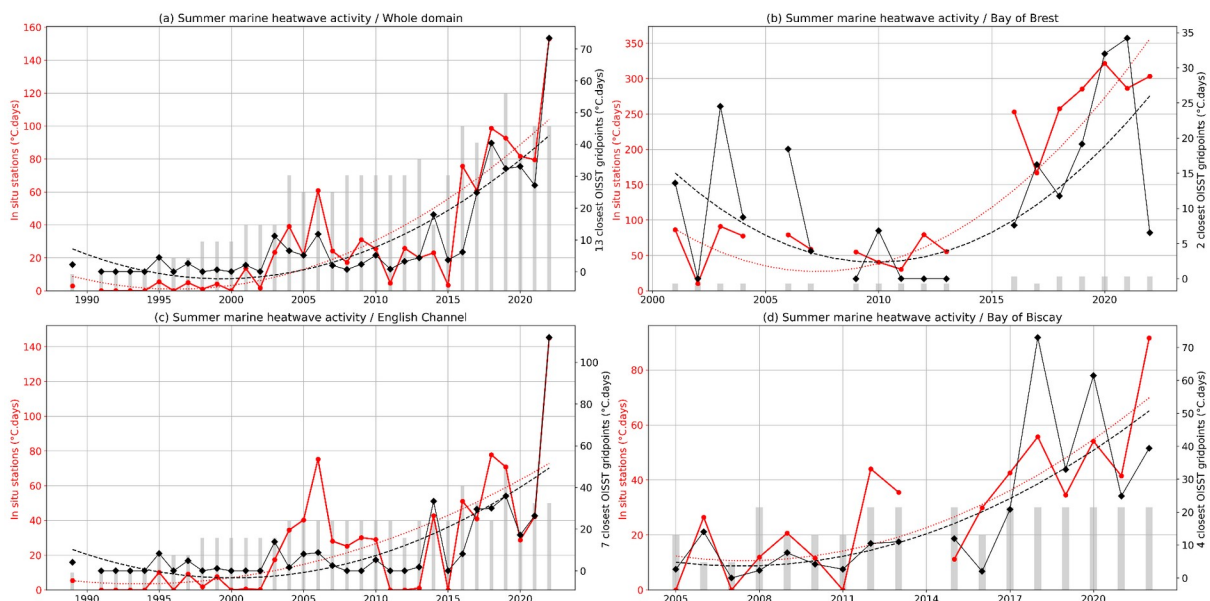
365 The spatial heterogeneity of the MHWs occurrence and activity can influence the  
366 impact of MHWs along the coastline. We now explore MHWs activity detected along the  
367 coast from *in situ* observations compared with remotely sensed observations. Figure 4 shows  
368 the activity detected for the whole northeast Atlantic domain and in the three subregions  
369 where long-term *in situ* observations exist. To compare *in situ* and satellite data, for each  
370 station, time series based on satellite data consider only years where *in situ* data exists (see  
371 Table S1 for the starting date) and exceeds 80% of available data for the considered season.  
372 Linked with the whole domain activity (Figure 4a), we observe an increase in the MHWs  
373 activity in the three subregions (Figure 4b, c, d). Similar evolutions are observed when the  
374 satellite product or coastal buoys are considered. In the Bay of Brest, we also observe a  
375

376 similar increase but with larger activity in *in situ* observation as the intensity of extreme is  
 377 underestimated by the satellite in this semi-enclosed bay. The use of *in situ* observation is  
 378 limiting the length of the analyzed time series. However, we can observe larger activity in  
 379 recent years from both datasets. For most cases, similar most active years are detected with *in*  
 380 *situ* observations and satellite data.

381 Considering coastal stations over the observed periods, we see a more pronounced  
 382 increase in MHWs activity from 2010. The English Channel and the Bay of Biscay *in situ*  
 383 stations highlight the year 2022 as the most active year exceeding 140 °C.days. In the Bay of  
 384 Brest, the impact of the 2022 MHWs is less pronounced, in agreement with satellite  
 385 observation (Figure 2b) due to tidally driven vertical mixing.

386 When we compare MHWs activity estimated from *in situ* stations and satellite product, values  
 387 are generally larger from *in situ* stations. Those differences are explained by the  
 388 underestimation of extreme temperatures in coastal regions in remotely sensed products.  
 389

390



391 Figure 4: Time series of summer (JJAS) MHWs mean activity (a) in the whole domain  
 392 (northeast Atlantic) and in three subregions: (b) Bay of Brest, (c) the English Channel, and (d)  
 393 Bay of Biscay. The red curve with circle marks represents the activity based on *in situ*  
 394 observations. The black curve with diamond marks represents the activity based on satellite  
 395 dataset for the closest non-masked points with *in situ* stations when *in situ* data exists. Dash  
 396 lines represent the regression of a third-order polynomial of the solid line with the same color.  
 397 Grey bars are proportional to the number of considered *in situ* time series. MHWs activity  
 398 from *in situ* time series with less than 80% of observation during the analyzed season is not  
 399 computed.  
 400

401

## 402 3.2 Evolution of marine cold-spell activity

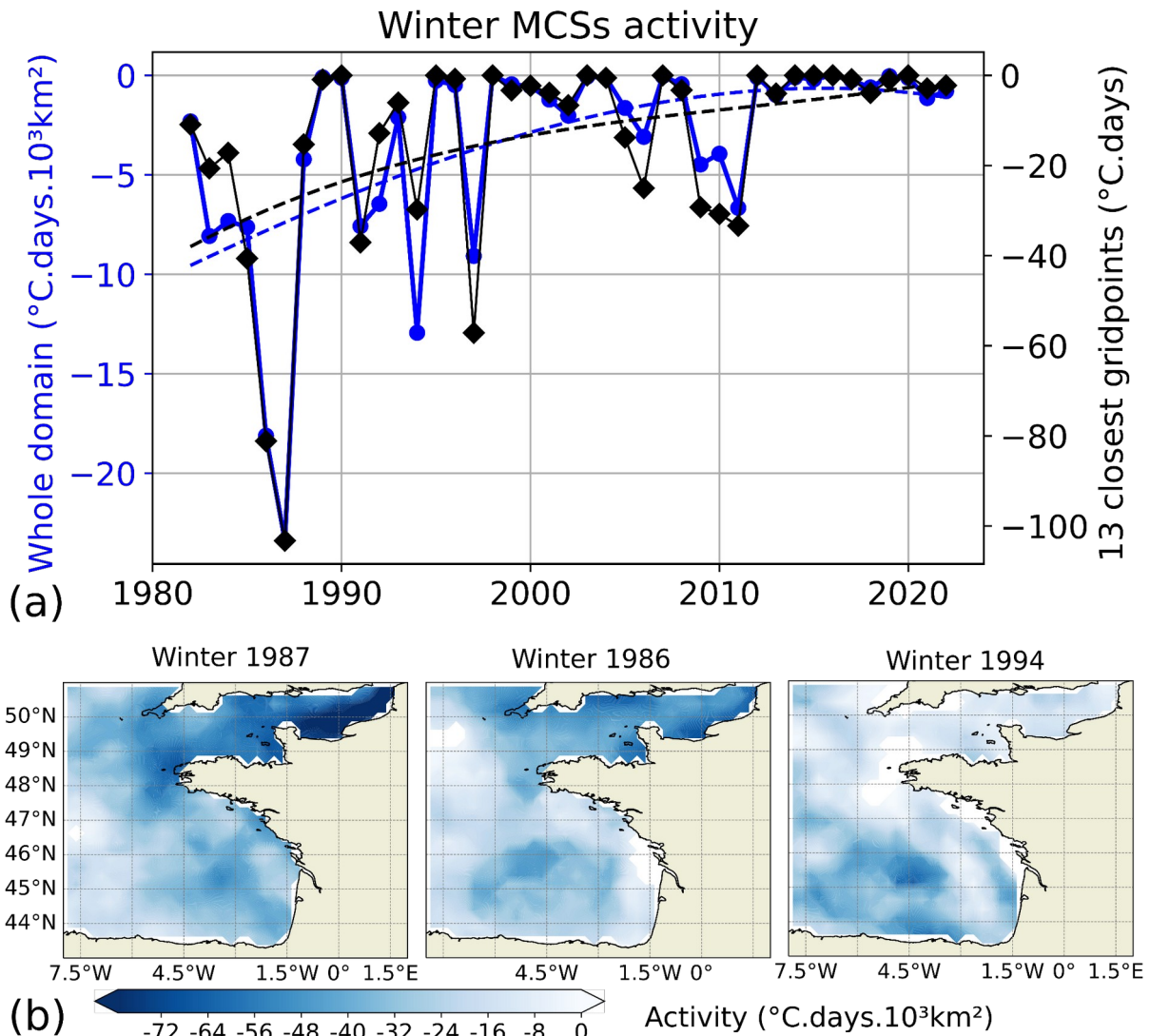
403

### 404 3.2.1 An integrated regional view

405

406

407



408  
409 Figure 5: Same as Figure 2 but for MCSs in winter (DJFM).  
410

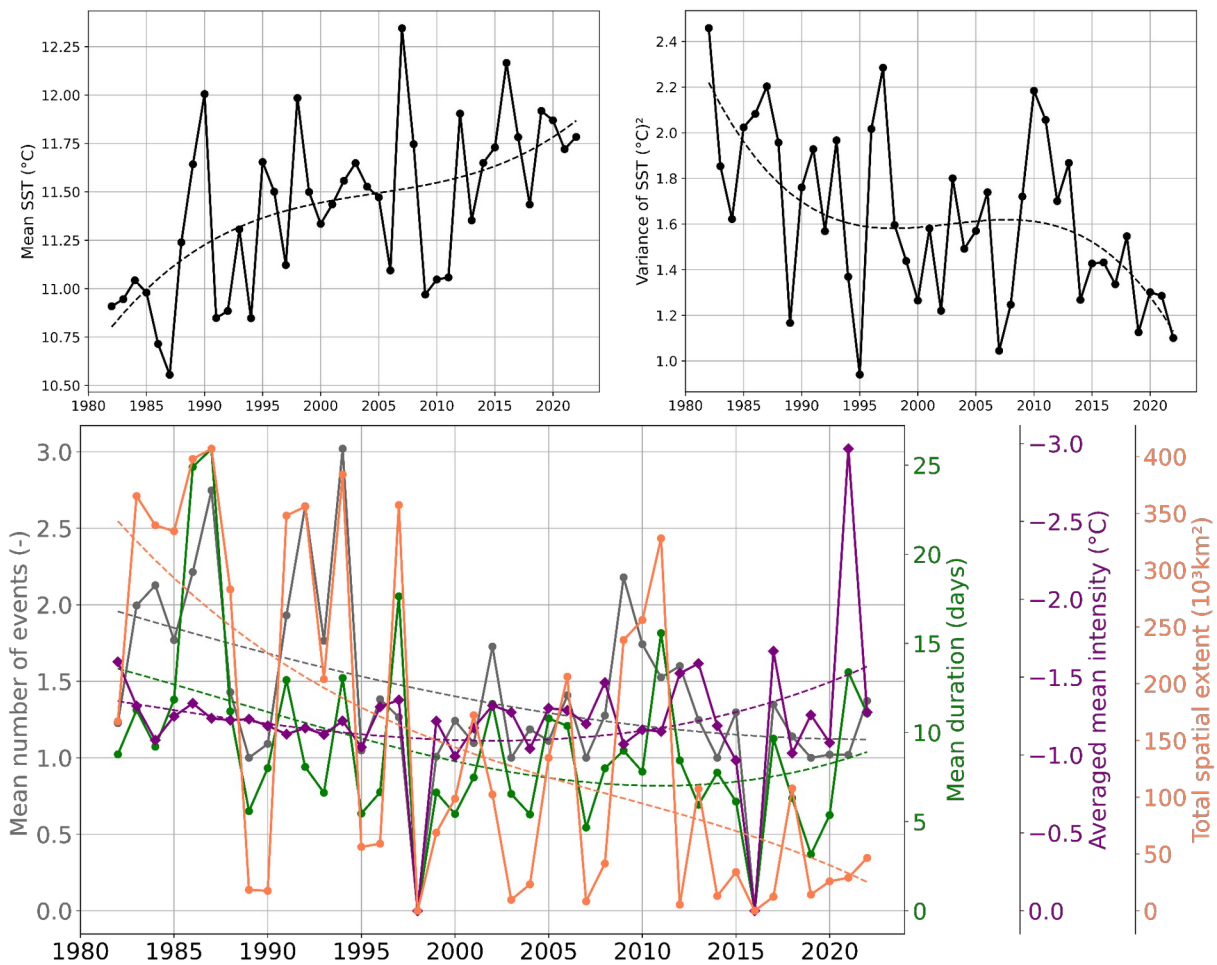
411 Figure 5 depicts winter MCSs evolution for the whole domain over the last four  
412 decades (1982-2022). MCSs activities decrease linearly during the first half of the period,  
413 showing almost no occurrence after 2000 with the exception of 2006 and 2009 to 2011. A  
414 similar evolution is seen by considering the average of the 13 grid points closest to each *in*  
415 *situ* station.  
416

417 The three most active MCSs occur in winter 1987 ( $-24\text{ }^{\circ}\text{C.days}\cdot 10^3\text{km}^2$ ), 1986 ( $-18$   
418  $^{\circ}\text{C.days}\cdot 10^3\text{km}^2$ ) and 1994 ( $-13\text{ }^{\circ}\text{C.days}\cdot 10^3\text{km}^2$ ). In the two coldest winters, MCSs were  
419 dominant in the English Channel, especially off the northern French Coast in winter 1987.  
420 These two winters are characterized by long ( $\sim 50$  days) and intense ( $\sim -2.5\text{ }^{\circ}\text{C}$  anomalous  
421 SST) and few events ( $\sim 1$  event; Figure S4). This region is subject to high turbulent mixing  
422 generated by the tidal current, which could favor cold conditions. By contrast to these two  
423 winters (1987 and 1986), winter 1994 featured strong MCSs activity in the center of the Bay  
424 of Biscay, due to numerous ( $\sim 5$  events) but moderate intensity ( $\sim -1.3\text{ }^{\circ}\text{C}$ ) and relatively short  
425 (20 days) events. The three winters 2009-2011 present very localized extreme cold conditions  
426 along the coastal Armorican Shelf, and additionally in the English Channel for 2011 (not  
427 shown). The detailed mean features (number of events, duration and mean intensity) of winter

428 MCSs over the period 1982-2022 in the northeast Atlantic, English Channel, Bay of Brest and  
 429 Bay of Biscay are documented in Table S3.

430

431



432

433

434 Figure 6: Same as Figure 3 but in winter (DJFM) and MCSs (blue curve)

435

436

437

438

439

440

441

442

The mean and variance evolution of SST, as well as the mean evolution of MCSs properties (occurrence, duration, mean intensity and spatial extent) are presented over the whole domain (Figure 6) and separately for the English Channel, the Bay of Brest and the Bay of Biscay (Figure S5). Over the whole northeast Atlantic domain, the SST mean increases and spatial dispersion (variance) decreases with both showing a plateau around 1995-2010, following the English Channel and the Bay of Biscay evolution. On the contrary, a steady increase in the mean SST and a nearly constant variance of SST is seen in the Bay of Brest.

443

444

445

446

447

448

The warmer winter seen over the whole domain and for the three subregions is consistent with the decrease of the extremely cold conditions, depicted by the mean MCSs activity. The decrease in the mean MCSs activity is controlled by the strong decrease in spatial extent (350 to 50  $\times 10^3 \text{ km}^2$ ), the moderate decrease in the number of events (2 to 1.2 events), and the small decrease in duration (13 to 9 days). The mean intensity does not show any trend ( $\sim -1.5 \text{ }^\circ\text{C}$ ).

449

450

451

The decrease of spatial dispersion (variance) of SST over the whole domain indicates a more uniform evolution which is explained by a dominant warming trend stronger for colder areas. Indeed, the relatively cold English Channel's temperature increased by 1.5  $^\circ\text{C}$  (from 9

452 °C to 10.5 °C) and the relatively warmer Bay of Biscay increased by 0.8 °C (from 11.8 °C to  
 453 12.6 °C) over the 1982-2022 period. When considering individually the three subregions,  
 454 localized enough to be under a similar trend, the variance also decreases (Figure S5). The  
 455 decrease of variance is more pronounced for the English Channel than for the Bay of Brest  
 456 and Bay of Biscay. Therefore, a first estimate shows that mean SST warming and the variance  
 457 changes both contribute to the changes in MCSs activity in the English Channel, Bay of Brest  
 458 and Bay of Biscay.

459 MCSs activity generally follows the SST evolution, albeit with small differences.  
 460 Indeed, winter 1991 and 1994 have a similar mean SST (10.8 °C) but the MCSs activity is  
 461 three times higher in 1994 than in 1991, driven by a higher number of events (3 instead of 2  
 462 events with similar duration, mean intensity and spatial extent).

463 Even if changes in winter occur in the Bay of Brest and Bay of Biscay, more drastic  
 464 changes are seen in the English Channel over the period 1982-2022 (see trend in Figure S6).  
 465 In the English Channel, the trend of MCSs shows at the beginning of the period, a mean  
 466 occurrence of 2 events/winter, lasting 15 days with a mean intensity of -1.5 °C over an area of  
 467  $100 \times 10^3 \text{ km}^2$ , followed by a sharp decline ending to no detected MCSs in the last four years  
 468 (2019-2022). In the Bay of Brest over the same period, MCSs properties decrease from 1.5  
 469 events during 15 days at a mean intensity of -1.4 °C over  $11 \times 10^3 \text{ km}^2$  to 0.5 events during 8  
 470 days at a mean intensity of -0.8 °C over  $0.5 \times 10^3 \text{ km}^2$ . Exceptional long events occurred in the  
 471 winter of 1987 with a mean duration of 55 days. In the Bay of Biscay, the MCSs decline in  
 472 occurrence (from 2 to 1 event), duration (from 11 to 9 days) and spatial extent ( $170$  to  $40 \times 10^3$   
 473  $\text{km}^2$ ) while the mean intensity rises from -1.3 °C to -1.5 °C. The increase is explained by  
 474 winter 2021; without these events, the mean intensity would have been nearly constant around  
 475 -1.3 °C. Indeed, winter 2021 shows a small activity but the highest mean intensity (-3 °C over  
 476 the whole domain) which is explained by a localized event in the coastal area off  
 477 southwestern France with a maximum intensity of (-5.6 °C). Apart from a very intense and  
 478 localized event in the coastal area off southwestern France in winter 2021 and a very long  
 479 event in the Bay of Brest in winter 1987, severe MCSs occurred predominantly in the English  
 480 Channel (winter 1987 and 1986).

481

482

### 483 3.2.2. Coastal MCSs activity

484

485 Figure 7 shows the time series of MCSs activity for *in situ* data and satellite data  
 486 considering the same missing data as each *in situ* station data. Along the coasts, MCSs  
 487 activity as determined by local buoys remains weaker than MHWs activity as defined using  
 488 satellite data. As for the MHWs, MCSs intensity is underestimated in satellite observations  
 489 but evolutions are similar. From *in situ* observations from coastal stations, two years can be  
 490 highlighted due to their intense MCSs: 2006 and 2010 (Figure 7). The year 2010 is the most  
 491 intense, in terms of MCSs. The mean activity is reaching -100 °C.day in the Bay of Brest and  
 492 around -60 °C.day in the Bay of Biscay and the English Channel. In 2006, the activity was  
 493 also important compared with other years: around -80 °C.day in the Bay of Brest and around -  
 494 50 °C.day in the English Channel. This extreme year 2006 was also unique with a peak in  
 495 MHWs activity during the summer (Figure 4). Before the year 2000, two other years reveal  
 496 intense MCSs activity in the coastal English Channel: 1997 and 1991 (from the most intense  
 497 to the less active winter).

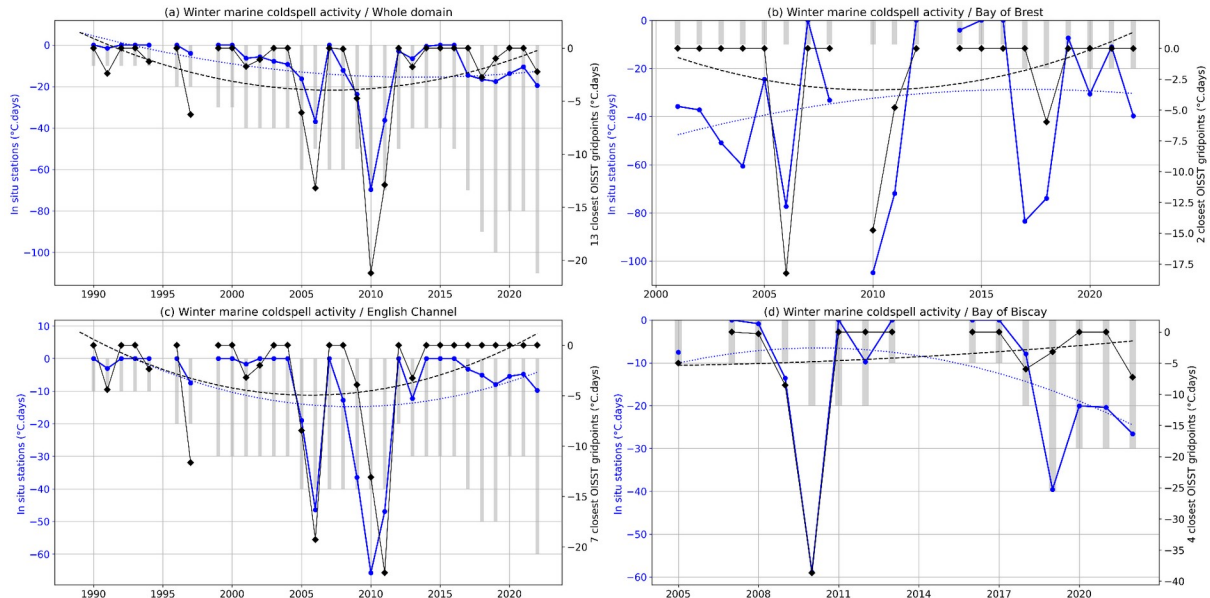
498 We do not detect a significant trend in the interannual evolution of MCSs activity  
 499 along the coasts. For the Bay of Biscay and the Bay of Brest, it can be directly connected to

500 the lack of observation before 2000 when the largest MCS occurs. In the English Channel, the  
 501 lack of observation also explains the lack of a clear trend. Indeed, only one time series was  
 502 available before 1995 and this station (GREENwich) is not detecting an important MCSs  
 503 activity before 2000.

504

505

506



507

508 Figure 7: Same as Figure 4 but for MCSs in winter (DJFM).

509

### 510 3.3 Associated atmospheric patterns

511

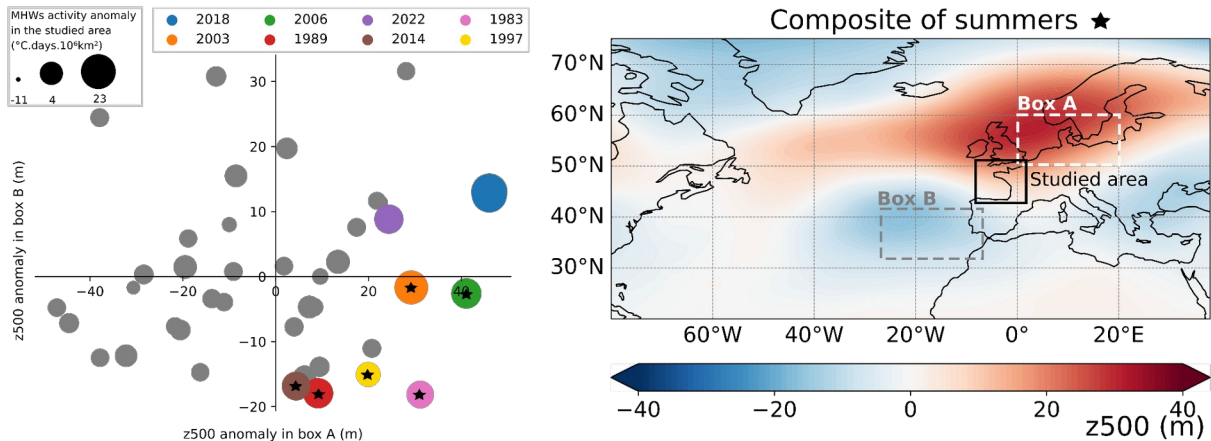
512 Apart from the long-term trend of increasing SST, we also see high interannual  
 513 variability which is potentially connected with atmospheric forcing modes (Holbrook et al.  
 514 2019; Izquierdo et al., 2022a). Figure 8 presents the atmospheric circulation in the north  
 515 Atlantic associated with strong interannual MHWs in the Bay of Biscay and the English  
 516 Channel. For each summer of the 1982-2022 period, MHWs total activity anomaly in the  
 517 studied area box (northeast Atlantic) with respect to the third-order long-term trend (red  
 518 dotted curved in Figure 2a) was computed. This anomaly represents the detrended or  
 519 interannual MHWs activity. Eight summers were identified as having high interannual  
 520 activities (anomalous total activity exceeding a threshold of  $4 \text{ } ^\circ\text{C}\cdot\text{days}\cdot 10^6\cdot\text{km}^2$ , coloured  
 521 marker in Figure 8 left panel). The year 2018 ( $23 \text{ } ^\circ\text{C}\cdot\text{days}\cdot 10^6\cdot\text{km}^2$ ), 2003 ( $17$   
 522  $^\circ\text{C}\cdot\text{days}\cdot 10^6\cdot\text{km}^2$ ) and 2006 ( $12 \text{ } ^\circ\text{C}\cdot\text{days}\cdot 10^6\cdot\text{km}^2$ ) are the three strongest summers. Six out of  
 523 these eight summers (all except 2018 and 2022) have an anomalous geopotential height at 500  
 524 hPa which is positive over northern Europe (box A in Figure 8) and negative west of the  
 525 Iberian Peninsula (box B in Figure 8). The composite of the anomalous geopotential height at  
 526 500 hPa for these six summers shows in the north Atlantic-Europe sector a positive summer  
 527 NAO-like pattern, with a high over the Nordic sea and two lows over the Iberian Peninsula  
 528 and Greenland. This overall result is not sensitive to small displacements of boxes (a few  
 529 latitude and longitude degrees; not shown).

530

531

532

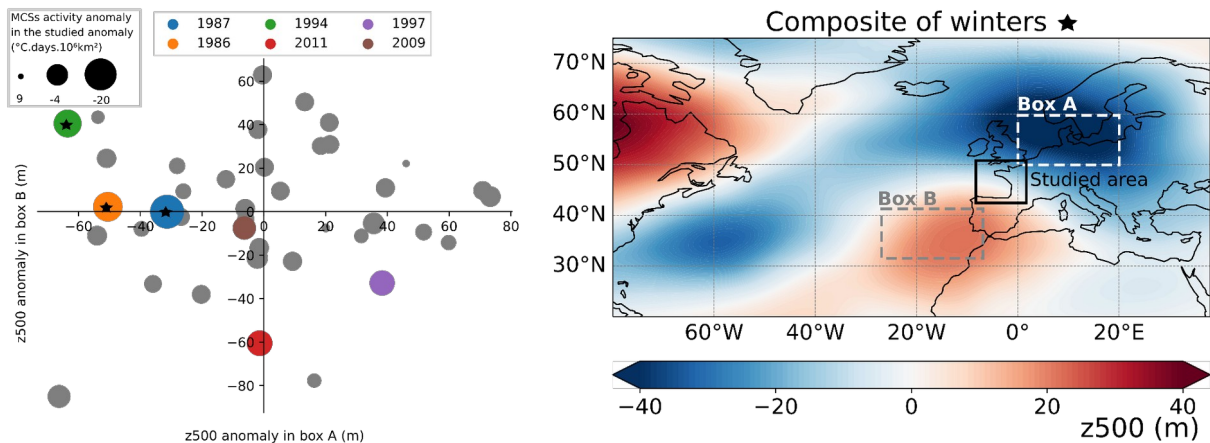
533



534  
 535 Figure 8: (Left panel) Scatter plot of anomalous summer (JJAS) geopotential height at 500  
 536 hPa (z500; in m) in box A versus the anomalous geopotential height at 500 hPa in box B with  
 537 respect to the summer period 1982-2022. The size of the marker is proportional to the  
 538 anomalous summer (JJAS) MHWs total activity, calculated as the sum of all grid point  
 539 activity in the studied area (in  $^{\circ}\text{C}\cdot\text{days}\cdot 10^6\cdot\text{km}^2$ ) with respect to the trend (red dotted curved in  
 540 Figure 2a). Markers are in color when this value exceeds  $4\text{ }^{\circ}\text{C}\cdot\text{days}\cdot 10^6\cdot\text{km}^2$  and the stars are  
 541 indicated when markers in color are in the lower-right “cluster” of the graph. (Right panel)  
 542 Composites of summers (JJAS) marked with stars in the left panel of the anomalous  
 543 geopotential height at 500 hPa (m) with respect to the summer period 1982-2022. Box A is  
 544 the domain  $0^{\circ}\text{E}$  to  $20^{\circ}\text{E}$ - $50^{\circ}\text{N}$  to  $60^{\circ}\text{N}$  and box B is the domain  $33^{\circ}\text{W}$  to  $13^{\circ}\text{W}$  -  $31^{\circ}\text{N}$  to  
 545  $41^{\circ}\text{N}$ .

546  
 547 Summer (JJAS) 2018 has the strongest anomalous MHWs activity in the northeast  
 548 Atlantic but, differently to the six next summers in the ranking of detrended MHWs activity,  
 549 does not present a decrease in the geopotential height at 500 hPa west of the Iberian Peninsula  
 550 (box B). A broad high-pressure system in the north Atlantic-European sector is seen  
 551 (including box A), except in the eastern Mediterranean and to  $60^{\circ}\text{N}$  where a low occurs  
 552 (Figure S7). This response in box B for summer 2018 is primarily due to late summer (August  
 553 and September) atmospheric circulation (Figure S7). These months have a minor contribution  
 554 to MHWs total activity for the whole summer (JJAS; Figure S8). When considering the month  
 555 of June, with 2018 MHWs peaks (Figure S8), the north Atlantic shows a positive summer  
 556 NAO regime, similar to the next six summers' highest MHWs activity. This analysis  
 557 demonstrates that MHWs in the northeast Atlantic is closely associated with a high-pressure  
 558 system over northern Europe, and a low off the Iberian Peninsula, resembling the positive  
 559 phase of the summer NAO. By performing this analysis with SST instead of MHWs activity,  
 560 we obtain similar results, albeit with a less extended high over northern Europe (Figure S9).  
 561

562



563  
 564 Figure 9: Same as Figure 8 but for MCSs in winter (DJFM). MCSs anomalies are calculated  
 565 with respect to the third-order trend (blue dotted curved in Figure 5). Markers are in color  
 566 when this value is below  $-4 \text{ }^{\circ}\text{C.days.10}^6.\text{km}^2$  and stars are indicated when markers in color  
 567 are in the upper-left section of the graph.

568 Regarding MCS, the three highest detrended MCSs activities are winter 1987 ( $-20$   
 569  $^{\circ}\text{C.days.10}^6.\text{km}^2$ ), 1986 ( $-13 \text{ }^{\circ}\text{C.days.10}^6.\text{km}^2$ ) and 1994 ( $-10 \text{ }^{\circ}\text{C.days.10}^6.\text{km}^2$ ; Figure 9).  
 570 These three most active winters are in the same “cluster”, with anomalous 500 hPa  
 571 geopotential height negative over northern Europe and positive west of the Iberian Peninsula.  
 572 Composite of the anomalous geopotential height at 500 hPa for these three winters shows in  
 573 the north Atlantic-Europe sector a broad and strong low in northern Europe, a weaker low-  
 574 pressure system sitting in the northwest Atlantic, and two highs off the Iberian Peninsula and  
 575 over the Hudson Bay. This analysis suggests that extreme MCSs in the northeast Atlantic  
 576 might be closely associated with a low over northern Europe and a high off the Iberian  
 577 Peninsula. By performing this analysis with SST instead of the MCSs activity (Figure S10),  
 578 the result are sparse, showing only winter 1986 as strong anomalous cold SST linked to an  
 579 anomalous geopotential height at 500 hPa over northern Europe and positive west of the  
 580 Iberian Peninsula.

581 When comparing the anomalous geopotential height conditions for the most intense  
 582 summer MHWs and winter MCS, we see that the geopotential height conditions are opposite,  
 583 although the amplitude is stronger for winter, consistent with stronger climatology (Folland et  
 584 al., 2009). However, while summer MHWs are associated with a positive summer NAO,  
 585 winter MCSs are not associated with a negative winter NAO pattern.

586 To investigate potential drivers of these events, we have considered the different  
 587 components of air-sea heat flux anomalies concomitant with MHWs and MCSs. For the eight  
 588 most severe interannual summer MHWs (see marker in color Figure 8) and the six most  
 589 severe interannual winter MCSs (see marker in color Figure 9), the anomalous (i) short-wave  
 590 radiation flux, (ii) surface net long-wave radiation flux, (iii) surface sensible heat flux and (iv)  
 591 latent heat flux are depicted, respectively Figure S11 and Figure S12. The interannual (or  
 592 detrended) summer MHWs are predominantly driven by high short-wave radiation flux,  
 593 except for years 1983 and 1997 that only shows important positive downward latent heat flux.  
 594 The other air-sea fluxes have a smaller contribution. The interannual winter MCSs seem to be  
 595 mostly driven by high sensible heat flux and low short-wave radiation flux. This suggests that,  
 596 in this region, a decrease in cloud cover is a key parameter for the generation of summer  
 597 MHWs while strong winds and an increase in cloud cover are important for the apparition of



598 winter MCSs. Further analysis needs to be done to attribute quantitatively the contribution of  
599 each air-sea heat flux component.

## 600 **4. Discussion**

601

602 In the northeast Atlantic, an increase in the MHWs activity and a decrease in MCSs  
603 activity were observed. Interannual changes confirm that general large scale trends (Oliver et  
604 al., 2018; Schlegel et al., 2021) are also observed in regions where the coastal hydrodynamics  
605 could limit the impact due to active vertical mixing processes (*e.g.* barotropic and internal  
606 tides, wind-driven mixing in shallow waters).

607 The most active summer MHWs analyzed over the northeast Atlantic and in the period  
608 1982-2022 occurred in the Bay of Biscay (2018) and the most active winter MCSs occurred in  
609 the English Channel (1987). This is consistent with Schlegel et al. (2021) who found that the  
610 maximum intensity of MHWs dominates MCSs in the Bay of Biscay, and vice versa in the  
611 English Channel. Along the coasts, the maximum of MHWs activity is detected in 2022 in the  
612 English Channel which might be related to the summer European heatwaves recorded  
613 (ECMWF, 2022; Savu, 2022; Guinaldo et al., 2023).

614 In the Bay of Biscay, we see a linear warming rate in summer since the beginning of  
615 the studied period. This is in accordance with DeCastro et al. (2009) which shows a steady  
616 linear warming rate since the 1970s, based on data from 1854-2006. Mean SST together with  
617 SST variance increase may explain the increase of MHW. This increase of MHWs is  
618 consistent with Izquierdo et al. (2022a) who determined more precisely an equal contribution  
619 of each of these two factors for the South coast of the Bay of Biscay. This is specific to this  
620 region (as well as for the Bay of Brest and the English Channel), as for most of the other  
621 regions of the world, the mean warming and not the SST variability changes contribute to the  
622 increase in MHWs features (Alexander et al., 2018; Oliver et al., 2020). In addition, we found  
623 a positive trend for the MHWs activity parameter using both satellite data and the 4 buoys in  
624 the Bay of Biscay, and for the duration and occurrence using satellite data. The trends are  
625 quasi-similar considering only the two buoys on the South coast of the Bay of Biscay (GIJO  
626 and BILB) and the two on the west coast of the Bay of Biscay (ARCA and MOLI; not shown)  
627 and are marked by the high activity present in the more recent summers. This evolution in the  
628 occurrence and duration of MHWs were not seen in Izquierdo et al. (2022b) using two buoys  
629 in the South coastal Bay of Biscay over the period 1998-2018, which could be explained by  
630 local process or studied season (March to August).

631

632 The results from *in situ* and satellite datasets for each of the studied regions are quite  
633 in agreement, albeit the satellite underestimates the amplitude of activity for both MHWs and  
634 MCS. Conversely, Izquierdo et al. (2022a) found an overestimation of the MHWs using  
635 satellites compared to *in situ* in the coastal upwelling region South of the Bay of Biscay,  
636 which might be related to local processes. The satellite's coarse resolution mostly (i) smoothes  
637 small-scale and short events and (ii) interpolates with offshore regions, having greater thermal  
638 inertia (Marin et al., 2021) which can lead to the overestimation of the duration of events and  
639 the underestimation of the intensity. However, we show that coastal *in situ* stations distributed  
640 along the northeast Atlantic coasts allow the detection of large-scale evolutions of MHWs and  
641 MCSs activity. Analyzed locally, they can also inform on evolutions related to local  
642 hydrodynamics.

643

644 Internal variability of winter MCSs is related to low pressure over northern Europe  
645 and a high-pressure West of the Iberian Peninsula for three (1987, 1986 and 1994) out of the  
646 six most intense events. Among other strong interannual MCSs, winter 2011 does not present

647 this pattern but could have been generated by a cold air outbreak brought by a ridge over  
648 Greenland (Norris et al., 2013). A relation at an interannual timescale could exist between  
649 MCSs (Figure 7, middle panel) and extreme low-salinity events (Poppeschi et al., 2021) in  
650 winter in the Bay of Brest, as, using the same *in situ* buoys (COAST-HF-Iroise from 2000-  
651 2018), two out of the four most severe low-salinity events are concomitant with MCSs (winter  
652 2001 and 2007). These extreme events could be both influenced by intense mid-latitude  
653 depressions, but river discharges are also an important driver in this region. Unlike MHWs  
654 (Figure 2), extreme cold conditions occurred several winters in a row: three in 2009-2011 and  
655 two in 1986-1987. This might be explained by the re-emergence of cold water originating  
656 from the previous winter, as for the 2013-2016 north Atlantic cold Blob (Duchez et al., 2016a;  
657 Josey et al., 2018; Schlegel et al., 2021).

658  
659 Summer 2018 presents the most active MHWs in the northeast Atlantic for the period  
660 1982-2022, consistent with the reported warmer SST the same summer (+1 to +3 °C above  
661 the long-term climatology) in the proximity of the United Kingdom (McCarty et al., 2019).  
662 Over land, this summer was also recorded as the hottest in the United Kingdom since 1884  
663 (McCarty et al., 2019) and one of the hottest over northwestern Europe (Met Office, 2018;  
664 Météo-France, 2018). On top of the underlying warming climate forcing (Vogel et al., 2019;  
665 Yiou et al., 2020), this extreme continental warm conditions in 2018 have been previously  
666 reported as a consequence of the positive summer NAO anomalies combined with elevated  
667 SST (McCarty et al., 2019) or combined with stationary Rossby waves in synoptic anomalies  
668 (Drouard et al., 2019; Kornhuber et al., 2019). More generally, the positive phase of the  
669 summer NAO is associated with warm anomalies from the west of the United Kingdom to the  
670 Baltic (Folland et al., 2009). Our findings for MHWs corroborate the continental counterpart  
671 as extremely warm conditions in the Bay of Biscay and the English Channel are likely  
672 associated with positive summer NAO, consistent with the result of Holbrook et al. (2019).

673  
674 Depending on the region and the event, MHWs can be associated with anomalous air–  
675 sea heat fluxes which can include high short-wave fluxes, due to less cloud cover and greater  
676 insolation, high sensible heat fluxes when the surface air is warm and/or low latent heat loss  
677 from the ocean, due to weak winds (Oliver et al., 2021). In the English Channel and the Bay  
678 of Biscay, Guinaldo et al. (2023) linked the summer of 2022 sea-surface temperature to  
679 abnormally high short-wave radiation in the Bay of Biscay and English Channel. In this study,  
680 a similar conclusion is found by considering the eight most severe interannual MHWs in the  
681 northeast Atlantic (which includes the English Channel and the Bay of Biscay, and summer of  
682 2022). Abnormally high short-wave radiation is likely associated with reduced cloudiness and  
683 Folland et al. (2009) have found that during the positive index phase of the summer NAO,  
684 northwest Europe experiences significantly reduced cloudiness. This is consistent with our  
685 suggestion that the positive phase of the summer NAO favours the generations of summer  
686 MHWs in the northeast Atlantic through reduced cloudiness. MCSs in the English Channel  
687 are associated with high sensible heat fluxes, consistent with reported MCSs often driven by  
688 strong winds in shallow waters, enabling a rapid cooling of the surface water (Crisp, 1964;  
689 Schlegel et al., 2021). We also found a possible role of weaker short-wave radiation, which  
690 might be related to increased cloud coverage.

691  
692 In the future and under increasing greenhouse gas concentrations, climate models  
693 predict that the ocean surface in the Bay of Biscay and the English Channel will continue to  
694 warm (Fox-Kemper et al., 2021) and a trend toward a positive summer NAO pattern (Faranda  
695 et al., 2019). Both these effects imply the long-term likelihood of increased MHWs in the  
696 northeast Atlantic, but to what extent are the long-term and the interannual variability

697 contributions remain to be shown. Also, the role of large-scale ocean circulation features,  
698 such as the Shelf Edge Current (Alheit et al., 2019) or Iberian Poleward Current (Charria et  
699 al., 2013), upper ocean preconditioning (Josey et al., 2018), and the importance of remote  
700 large-scale climate modes of variability, such as the Indian Ocean Dipole (Holbrook et al.,  
701 2019) in amplifying or suppressing MHWs occurrences in the Bay of Biscay and English  
702 Channel would need specific investigation. Along the coasts, the role of main river inflow at  
703 the land-sea continuum can also lead to specific answers on the coastal ocean to future climate  
704 evolutions.

705  
706

## 707 5. Conclusions

708

709 The activity index, a combination of the properties of marine extreme events, shows a  
710 positive trend for summer MHWs in the northeast Atlantic (since 2000 and more pronounced  
711 since 2010) and in the three subregions, the English Channel, the Bay of Brest and the Bay of  
712 Biscay for both *in situ* and satellite data. This is explained by both a mean and variance SST  
713 increase. Conversely, a decrease in MCSs activity was detected, with almost no events after  
714 2000, more clearly shown with the satellite data due to the longer time series (40 years)  
715 compared with the *in situ* (20 to 30 years). These changes are fast for the three subregions,  
716 with the English Channel being the subregion with the more drastic growth.

717 In the northeast Atlantic, MHWs are more frequent, longer, and extend over larger areas,  
718 while the opposite is seen for MCSs. For both MHWs and MCSs, the mean intensity shows  
719 only weak changes over the last four decades.

720 Moreover, we found that the satellite dataset used is in good accordance with *in situ* data in  
721 the northeast Atlantic, except for the fact that satellites underestimate the amplitude of both  
722 hot summer and cold winter marine extreme events in the coastal areas. The implemented *in*  
723 *situ* stations appear as a well-designed observing system to detect the long-term evolution of  
724 MHWs and MCSs activity and to document local features related to coastal hydrodynamics.

725

726 MHWs activity is particularly high in 2018 and 2022 through two different situations.  
727 The year 2018 is characterized by a large extent of MHWs in the Bay of Biscay with long  
728 events in the South of the Bay and intense events in the Armorican Shelf. The summer of  
729 2022 features long MHWs mainly in the English Channel. MCSs activity is the highest in  
730 1986 and 1987 due to long and intense events in the English Channel.

731 Our findings show that summers with strong MHWs activity due to internal variability  
732 (after removing the trend) in northeast Atlantic have often been associated with a ridge over  
733 the northern Europe sea and a trough west of the Iberian Peninsula; the opposite situation is  
734 seen for MCSs. In the case of MHW, the wide atmospheric pattern resembles the positive  
735 phase of the summer NAO. This preliminary analysis of air-sea heat fluxes suggests that in  
736 the northeast Atlantic interannual (or detrended) summer MHWs are predominantly driven by  
737 high short-wave radiation flux and interannual winter MCSs by high sensible heat flux and  
738 low short-wave radiation. This suggests that, in this region, decreased cloud cover is a key  
739 parameter for the generation of summer MHWs while strong winds and increased cloud cover  
740 is important for the apparition of winter MCSs. We caution that the proposed connection does  
741 not necessarily indicate causal links but these relations can provide indications of drivers.

742

743 Despite contrasting hydrodynamical regimes (meso- and macro-tidal) and circulation  
744 (shallow water under freshwater influence, shelf circulation, active sub-mesoscale), the  
745 northeast Atlantic region displays similar changes in MHWs and MCSs activity between

746 coastal and open ocean regions. Those changes need to be anticipated to mitigate the impacts  
747 on coastal ecosystems.  
748

## 749 **Acknowledgements**

750 This work was partially supported by national funds through FCT (Fundação para a  
751 Ciência e a Tecnologia, Portugal) through project ROADMAP (JPIOCEANS/0001/2019). It  
752 is also funded by the regional project (Contrat Plan Etat-Region) ObsOcean/ROEC-ILICO  
753 and the regional COXTCLIM project funded by the Loire-Brittany Water Agency, the  
754 Brittany region, and Ifremer. We thank Oregon Segalen for fruitful discussions. We thank  
755 Tim Smyth for providing data from Western Channel Observatory. We acknowledge the  
756 COAST-HF (<http://www.coast-hf.fr>) national observing network component of the National  
757 Research Infrastructure ILICO. Additionally, we express our gratitude to the two reviewers  
758 and editor for their valuable feedback, which has greatly contributed to improving the quality  
759 of our work.  
760

## 761 **Declaration of competing interest**

762 The authors declare that they have no known competing financial interests or personal  
763 relationships that could have appeared to influence the work reported in this paper.

## 764 **Authors contributions**

765 All authors contributed to the conception and design of the study. AS performed the  
766 calculation and designed the figures involving the satellite dataset, GC and CP did so for the  
767 *in situ* dataset. All authors contributed to the discussion, writing and review of the manuscript.  
768  
769

## 770 **References**

771  
772 Alexander, M. A., Scott, J. D., Friedland, K. D., Mills, K. E., Nye, J. A., Pershing, A. J., and  
773 Thomas, A. C.: Projected sea surface temperatures over the 21st century: Changes in the  
774 mean, variability and extremes for large marine ecosystem regions of Northern Oceans,  
775 *Elementa: Science of the Anthropocene*, 6, 2018.  
776  
777 Alheit, J., Gröger, J., Licandro, P., McQuinn, I. H., Pohlmann, T., and Tsikliras, A. C.: What  
778 happened in the mid-1990s? The coupled ocean-atmosphere processes behind climate-induced  
779 ecosystem changes in the Northeast Atlantic and the Mediterranean, *Deep Sea Research Part*  
780 *II: Topical Studies in Oceanography*, 159, 130-142,  
781 <https://doi.org/10.1016/j.dsr2.2018.11.011>, 2019.  
782

- 783 Barnston, A. G., and Livezey, R. E.: Classification, seasonality and persistence of low-  
784 frequency atmospheric circulation patterns, *Monthly weather review*, 115(6), 1083-1126,  
785 <https://doi.org/10.1175/1520-0493>, 1987.
- 786 Brown Ross, A., Lilley, M. K. S., Shutler, J., Widdicombe, C., Rooks, P., McEvoy, A.,  
787 Torres, R., Artioli, Y., Rawle, G., Homyard, J., Tyler, C. R., and Lowe, C.: Harmful Algal  
788 Blooms and their impacts on shellfish mariculture follow regionally distinct patterns of water  
789 circulation in the western English Channel during the 2018 heatwave, *Harmful Algae*, 111  
790 (December 2021), 102166, <https://doi.org/10.1016/j.hal.2021.102166>, 2022.
- 791 Charria, G., Lazure, P., Le Cann, B., Serpette, A., Reverdin, G., Louazel, S., Batifoulier, F.,  
792 Dumas, F., Pichon, A., and Morel, Y.: Surface layer circulation derived from Lagrangian  
793 drifters in the Bay of Biscay, *Journal of Marine Systems*, 109, 60–76,  
794 <https://doi.org/10.1016/j.jmarsys.2011.09.015>, 2013.
- 795 Chust, G., Borja, Á., Caballero, A., Irigoien, X., Sáenz, J., Moncho, R., Marcos, M., Liria, P.,  
796 Hidalgo, J., Valle, M., and Valencia, V.: Climate change impacts on coastal and pelagic  
797 environments in the southeastern Bay of Biscay, *Climate Research*, 48(2–3), 307–332,  
798 <https://doi.org/10.3354/cr00914>, 2011.
- 799 Crisp, D. J.: The Effects of the Severe Winter of 1962-63 on Marine Life in Britain. *Journal of*  
800 *Animal Ecology*, 33(1), 165-210, <https://www.jstor.org/stable/2355>, 1964.
- 801 Darmaraki, S., Somot, S., Sevault, F., and Nabat, P.: Past Variability of Mediterranean Sea  
802 Marine Heatwaves. *Geophysical Research Letters*, 46(16), 9813–9823,  
803 <https://doi.org/10.1029/2019GL082933>, 2019.
- 804 DeCastro, M., Gómez-Gesteira, M., Alvarez, I., and Gesteira, J. L. G.: Present warming  
805 within the context of cooling–warming cycles observed since 1854 in the Bay of Biscay,  
806 *Continental Shelf Research*, 29(8), 1053-1059, <https://doi.org/10.1016/j.csr.2008.11.016>,  
807 2009.
- 808
- 809 Deser, C., Alexander, M. A., Xie, S. P., and Phillips, A. S.: Sea surface temperature  
810 variability: Patterns and mechanisms, *Annual review of marine science*, 2, 115-143, 2010.
- 811
- 812 Drouard, M., Kornhuber, K., and Woollings, T.: Disentangling dynamic contributions to  
813 summer 2018 anomalous weather over Europe, *Geophysical Research Letters*, 46(21), 12537-  
814 12546, <https://doi.org/10.1029/2019GL084601>, 2019.
- 815 ECMWF: Update on European heatwave of July 2022 (available at:  
816 [www.ecmwf.int/en/about/media-centre/focus/2022/update-european-heatwave-july-2022](http://www.ecmwf.int/en/about/media-centre/focus/2022/update-european-heatwave-july-2022)),  
817 2022.
- 818 Faranda, D., Alvarez-Castro, M. C., Messori, G., Rodrigues, D., and Yiou, P.: The hammam  
819 effect or how a warm ocean enhances large scale atmospheric predictability, *Nature*  
820 *communications*, 10(1), 1-7, <https://doi.org/10.1038/s41467-019-09305-8>, 2019.

- 821 Folland, C. K., Knight, J., Linderholm, H. W., Fereday, D., Ineson, S., and Hurrell, J. W.: The  
 822 summer North Atlantic Oscillation: past, present, and future, *Journal of Climate*, 22(5), 1082-  
 823 1103, 2009.
- 824 Fox-Kemper, B., Hewitt, H.T., Xiao, C. , Aðalgeirsdóttir, G., Drijfhout, S.S., Edwards, T.L.,  
 825 Golledge, N.R., Hemer, M., Kopp, R.E., Krinner, G., Mix, A., Notz, D., Nowicki, S., Nurhati,  
 826 I.S., Ruiz, L., Sallée, J.-B., Slangen, A.B.A., and Yu, Y.: Ocean, Cryosphere and Sea Level  
 827 Change, in *Climate Change 2021: The Physical Science Basis. Contribution of Working*  
 828 *Group I to the Sixth Assessment Report of the Intergovernmental Panel on Climate Change*  
 829 [Masson-Delmotte, V., Zhai, P., Pirani, A., Connors, S.L., Péan, C., Berger, S., Caud, N.,  
 830 Chen, Y., Goldfarb, L., Gomis, M.I., Huang, M., Leitzell, K., Lonnoy, E., Matthews, J.B.R. ,  
 831 Maycock, T.K., Waterfield, T., Yelekçi, O., Yu, R. and Zhou, B. (eds.)]. Cambridge  
 832 University Press, Cambridge, United Kingdom and New York, NY, USA, 1211–1362,  
 833 <https://doi.org/10.1017/9781009157896.011>, 2021.
- 834
- 835 Frölicher, T. L., Fischer, E. M., and Gruber, N.: Marine heatwaves under global warming,  
 836 *Nature*, 560(7718), 360-364, <https://doi.org/10.1038/s41586-018-0383-9>, 2018.
- 837 Frölicher, T., and Laufkötter, C.: Emerging risks from marine heat waves, *Nature*  
 838 *Communications*, 9(1), 2015–2018, <https://doi.org/10.1038/s41467-018-03163-6> , 2018.
- 839 Gómez, F., and Souissi, S.: The impact of the 2003 summer heat wave and the 2005 late cold  
 840 wave on the phytoplankton in the north-eastern English Channel, *Comptes Rendus -*  
 841 *Biologies*, 331(9), 678–685, <https://doi.org/10.1016/j.crv.2008.06.005>, 2008.
- 842 Guinaldo, T., Voldoire, A., Waldman, R., Saux Picart, S., and Roquet, H.: Response of the sea  
 843 surface temperature to heatwaves during the France 2022 meteorological summer, *Ocean*  
 844 *Science*, 19(3), 629-647, 2023.
- 845
- 846 Guo, X., Gao, Y., Zhang, S., Wu, L., Chang, P., Cai, W., Zscheischler, J., Ruby Leung, L.,  
 847 Small, J., Danabasoglu, G., Thompson, L., and Gao, H.: Threat by marine heatwaves to  
 848 adaptive large marine ecosystems in an eddy-resolving model, *Nature climate change*, 12(2),  
 849 179-186, 2022.
- 850
- 851 Hersbach, H., Bell, B., Berrisford, P., Hirahara, S., Horányi, A., Muñoz-Sabater, J., Nicolas,  
 852 J., Peubey, C., Radu, R., Schepers, D., Simmons, A., Soci, C., Abdalla, S., Abellan, X.,  
 853 Balsamo, G., Bechtold, P., Biavati, G., Bidlot, J., Bonavita, M., De Chiara, G., Dahlgren, P.,  
 854 Dee, D., Diamantakis, M., Dragani, R., Flemming, J., Forbes, R., Fuentes, M., Geer, A.,  
 855 Haimberger, L., Healy, S., Hogan, R. J., Hólm, E., Janisková, M., Keeley, S., Laloyaux, P.,  
 856 Lopez, P., Lupu, C., Radnoti, G., de Rosnay, P., Rozum, I., Vamborg, F., Villaume, S., and  
 857 Thépaut, J. N.: The ERA5 global reanalysis, *Quarterly Journal of the Royal Meteorological*  
 858 *Society*, 146(730), <https://doi.org/10.1002/qj.3803>, 1999-2049, 2020.
- 859 Hobday, A. J., Alexander, L. V., Perkins, S. E., Smale, D. A., Straub, S. C., Oliver, E. C. J.,  
 860 Benthuyssen, J. A., Burrows, M. T., Donat, M. G., Feng, M., Holbrook, N. J., Moore, P. J.,

- 861 Scannell, H. A., Sen Gupta, A., and Wernberg, T.: A hierarchical approach to defining  
862 marine heatwaves, *Progress in Oceanography*, 141, 227–238,  
863 <https://doi.org/10.1016/j.pocean.2015.12.014>, 2016.  
864
- 865 Holbrook, N. J., Scannell, H. A., Sen Gupta, A., Benthuyssen, J. A., Feng, M., Oliver, E. C.,  
866 Alexander, L., Burrows, M., Donat, M., Hobday, A., Moore, P., Perkins-Kirkpatrick, S.,  
867 Smale, D., Straub, S., and Wernberg, T.: A global assessment of marine heatwaves and their  
868 drivers, *Nature Communications*, 10(1), 1-13, <https://doi.org/10.1038/s41467-019-10206-z>,  
869 2019.  
870
- 871 Huang, B., Liu, C., Banzon, V., Freeman, E., Graham, G., Hankins, B., Smith, T., and Zhang,  
872 H.-M.: Improvements of the Daily Optimum Interpolation Sea Surface Temperature  
873 (DOISST) Version 2.1, *Journal of Climate*, 34, 2923-2939, [https://doi.org/10.1175/JCLI-D-](https://doi.org/10.1175/JCLI-D-20-0166)  
874 20-0166, 2020.
- 875 Hurrell, J. W., Kushnir, Y., Ottersen, G., and Visbeck, M., An overview of the North Atlantic  
876 oscillation, *Geophysical Monograph-American Geophysical Union*, 134, 1-36,  
877 <https://doi.org/10.1029/134GM01>, 2003.
- 878 Izquierdo, P., Rico, J. M., Taboada, F. G., González-Gil, R., and Arrontes, J.: Characterization  
879 of marine heatwaves in the Cantabrian Sea, SW Bay of Biscay, *Estuarine, Coastal and Shelf  
880 Science*, 274, <https://doi.org/10.1016/j.ecss.2022.107923>, 2022a.
- 881 Izquierdo, P., Taboada, F. G., González-Gil, R., Arrontes, J., and Rico, J. M.: Alongshore  
882 upwelling modulates the intensity of marine heatwaves in a temperate coastal sea, *Science of  
883 the Total Environment*, 835, <https://doi.org/10.1016/j.scitotenv.2022.155478>, 2022b.
- 884 Joint, I., and Smale, D. A.: Marine heatwaves and optimal temperatures for microbial  
885 assemblage activity, *FEMS Microbiology Ecology*, 93(2), 1–9,  
886 <https://doi.org/10.1093/femsec/fiw243>, 2017.
- 887 Josey, S.A., Hirschi, J.-M., Sinha, B., Duchez, A., Grist, J.P., Marsh, R.: The recent Atlantic  
888 cold anomaly: Causes, consequences, and related phenomena, *Ann. Rev. Marine Sci.* 10 (1),  
889 475–501, 2018.
- 890 Kornhuber, K., Osprey, S., Coumou, D., Petri, S., Petoukhov, V., Rahmstorf, S., and Gray, L.:  
891 Extreme weather events in early summer 2018 connected by a recurrent hemispheric wave-7  
892 pattern, *Environmental Research Letters*, 14(5), 054002,  
893 <https://doi.org/10.1088/1748-9326/ab13bf>, 2019.  
894
- 895 Le Boyer, A., Cambon, G., Daniault, N., Herbette, S., Le Cann, B., Marie, L., and Morin, P.:  
896 Observations of the Ushant tidal front in September 2007, *Continental Shelf Research*, 29(8),  
897 1026-1037, 2009.  
898

- 899 Lima, F. P., and Wethey, D. S.: Three decades of high-resolution coastal sea surface  
900 temperatures reveal more than warming, *Nature communications*, 3(1), 704, 2012.  
901
- 902 Lorenzo, M. N., Taboada, J. J., and Gimeno, L.: Links between circulation weather types and  
903 teleconnection patterns and their influence on precipitation patterns in Galicia (NW Spain),  
904 *International Journal of Climatology: A Journal of the Royal Meteorological Society*, 28(11),  
905 1493-1505, <https://doi.org/10.1002/joc.1646>, 2008.  
906
- 907 Marin, M., Feng, M., Phillips, H. E., and Bindoff, N. L.: A global, multiproduct analysis of  
908 coastal marine heatwaves: Distribution, characteristics, and long-term trends, *Journal of*  
909 *Geophysical Research: Oceans*, 126(2), e2020JC016708, 2021.  
910
- 911 McCarthy, M., Christidis, N., Dunstone, N., Fereday, D., Kay, G., Klein-Tank, A., Lowe, J.,  
912 Petch, J., Scaife, A., and Stott, P.: Drivers of the UK summer heatwave of 2018. *Weather*,  
913 74(11), 390-396, <https://doi.org/10.1002/wea.3628>, 2019.
- 914 Met Office : Summer 2018,  
915 [https://www.metoffice.gov.uk/binaries/content/assets/metofficegovuk/pdf/weather/learn-](https://www.metoffice.gov.uk/binaries/content/assets/metofficegovuk/pdf/weather/learn-about/uk-past-events/interesting/2018/summer-2018---met-office.pdf)  
916 [about/uk-past-events/interesting/2018/summer-2018---met-office.pdf](https://www.metoffice.gov.uk/binaries/content/assets/metofficegovuk/pdf/weather/learn-about/uk-past-events/interesting/2018/summer-2018---met-office.pdf), 2018. Last accessed  
917 7/7/2023.
- 918 Météo-France: Bilan climatique de l'été 2018,  
919 [https://meteofrance.fr/sites/meteofrance.fr/files/files/editorial/Bilan-climatique-](https://meteofrance.fr/sites/meteofrance.fr/files/files/editorial/Bilan-climatique-annee2018.pdf)  
920 [annee2018.pdf](https://meteofrance.fr/sites/meteofrance.fr/files/files/editorial/Bilan-climatique-annee2018.pdf), 2018, Last accessed 7/7/2023.  
921
- 922 Mieszkowska, N., Burrows, M., and Sugden, H.: Impacts of climate change on intertidal  
923 habitats, relevant to the coastal and marine environment around the UK, *MCCIP Science*  
924 *Review 2020*, 256-271, <https://doi.org/10.14465/2020.arc12.ith>, 2020.
- 925 Müller, H., Blanke, B., Dumas, F., and Mariette, V.: Identification of typical scenarios for the  
926 surface Lagrangian residual circulation in the Iroise Sea. *Journal of Geophysical Research:*  
927 *Oceans*, 115(C7), 2010.
- 928 Norris, J., Vaughan, G., and Schultz, D. M.: Snowbands over the English Channel and Irish  
929 Sea during cold-air outbreaks, *Quarterly Journal of the Royal Meteorological Society*,  
930 139(676), 1747-1761, <https://doi.org/10.1002/qj.2079>, 2013.
- 931 Oh, H., Kim, G. U., Chu, J. E., Lee, K., and Jeong, J. Y. The record-breaking 2022 long-  
932 lasting marine heatwaves in the East China Sea, *Environmental Research Letters*, 18(6),  
933 064015, 2023.
- 934 Oliver, E. C., Donat, M. G., Burrows, M. T., Moore, P. J., Smale, D. A., Alexander, L. V.,  
935 Benthuisen, J. A., Feng, M., Sen Gupta, A., Hobday, A. J., Holbrook, N. J., Perkins-  
936 Kirkpatrick, S. E., Scannell, H. A., Strauband, S. C., and Wernberg, T.: Longer and more



- 937 frequent marine heatwaves over the past century, *Nature communications*, 9(1), 1-12,  
938 <https://doi.org/10.1038/s41467-018-03732-9>, 2018.
- 939 Oliver, E. C. J., Burrows, M. T., Donat, M. G., Sen Gupta, A., Alexander, L. V., Perkins-  
940 Kirkpatrick, S. E., Benthuyssen, J. A., Hobday, A. J., Holbrook, N. J., Moore, P. J., Thomsen,  
941 M. S., Wernberg, T., and Smale, D. A.: Projected Marine Heatwaves in the 21st Century and  
942 the Potential for Ecological Impact, *Frontiers in Marine Science*, 6(December), 1–12,  
943 <https://doi.org/10.3389/fmars.2019.00734>, 2019.
- 944
- 945 Plecha, S., and Soares, P. M. M.: Global marine heatwave events using the new CMIP6 multi-  
946 model ensemble: from shortcomings in present climate to future projections, *Environmental*  
947 *Research Letters*, 15 (12), 124058, <https://doi.org/10.1088/1748-9326/abc847>, 2020.
- 948 Plecha, S. M., Soares, P. M. M., Silva-Fernandes, S. M., and Cabos, W.: On the uncertainty of  
949 future projections of Marine Heatwave events in the North Atlantic Ocean, *Climate*  
950 *Dynamics*, 56, 2027–2056, <https://doi.org/10.1007/s00382-020-05529-3>, 2021.
- 951 Poppeschi, C., Charria, G., Goberville, E., Rimmelin-Maury, P., Barrier, N., Petton, S.,  
952 Unterberger, M., Grossteffan, E., Repecaud, M., Quemener, L., Theetten, S., Le Roux, J.-F.  
953 and Tréguer, P.: Unraveling salinity extreme events in coastal environments: A winter focus  
954 on the bay of brest. *Frontiers in Marine Science*, 8, 705403,  
955 <https://doi.org/10.3389/fmars.2021.705403>, 2021.
- 956
- 957 Poppeschi, C., Charria, G., Daniel, A., Verney, R., Rimmelin-Maury, P., Retho, M.,  
958 Goberville, E., Grossteffan, E., and Plus, M.: Interannual variability of the initiation of the  
959 phytoplankton growing period in two French coastal ecosystems, *Biogeosciences*, 19, 5667–  
960 5687, <https://doi.org/10.5194/bg-19-5667-2022>, 2022.
- 961
- 962 Reynolds, R. W., Smith, T. M., Liu, C., Chelton, D. B., Casey, K. S., and Schlax, M. G.:  
963 Daily high-resolution-blended analyses for sea surface temperature, *J. Clim.*, 20, 5473–96,  
964 2007.
- 965 Ruthrof, K. X., Breshears, D. D., Fontaine, J. B., Froend, R. H., Matusick, G., Kala, J., Miller,  
966 B. P., Mitchell, P. J., Wilson, S. K., van Keulen, M., Enright, N. J., Law, D. J., Wernberg, T.,  
967 and Hardy, G. E. S. J.: Subcontinental heat wave triggers terrestrial and marine, multi-taxa  
968 responses, *Scientific Reports*, 8(1), 1–9, <https://doi.org/10.1038/s41598-018-31236-5>, 2018.
- 969 Savu, A.: Temperature Highs, Climate Change Salience, and Eco-Anxiety: Early Evidence  
970 from the 2022 United Kingdom Heatwave, *Climate Change Salience, and Eco-Anxiety*, 2022.
- 971 Sims, D. W., Wearmouth, V. J., Genner, M. J., Southward, A. J., and Hawkins, S. J.: Low-  
972 temperature-driven early spawning migration of a temperate marine fish, *Journal of Animal*  
973 *Ecology*, 73(2), 333-341, 2004.
- 974 Smale, D. A., Wernberg, T., Oliver, E. C. J., Thomsen, M., Harvey, B. P., Straub, S. C.,  
975 Burrows, M. T., Alexander, L. V., Benthuyssen, J. A., Donat, M. G., Feng, M., Hobday, A. J.,

- 976 Holbrook, N. J., Perkins-Kirkpatrick, S. E., Scannell, H. A., Sen Gupta, A., Payne, B. L., and  
977 Moore, P. J.: Marine heatwaves threaten global biodiversity and the provision of ecosystem  
978 services, *Nature Climate Change*, 9(4), 306–312, <https://doi.org/10.1038/s41558-019-0412-1>,  
979 2019.
- 980 Seuront, L., Nicastro, K. R., Zardi, G. I., and Goberville, E.: Decreased thermal tolerance  
981 under recurrent heat stress conditions explains summer mass mortality of the blue mussel  
982 *Mytilus edulis*, *Scientific Reports*, 9(1), 1–14, <https://doi.org/10.1038/s41598-019-53580-w>,  
983 2019.
- 984 Schlegel R. W., E. C. J. Oliver, T. Wernberg, Smit, A. J.: Nearshore and offshore co-  
985 occurrence of marine heatwaves and cold-spells, *Progress in Oceanography*, 151, 189–205,  
986 <https://doi.org/10.1016/j.pocean.2017.01.004>, 2017.
- 987 Schlegel, R. W., Darmaraki, S., Benthuyzen, J. A., Filbee-Dexter, K., and Oliver, E. C. J.:  
988 Marine cold-spells, *Progress in Oceanography*, 198, 102684,  
989 <https://doi.org/10.1016/j.pocean.2021.102684>, 2021.
- 990 Simon, A., Plecha, S. M., Russo, A., Teles-Machado, A., Donat, M. G., Auger, P. A., and  
991 Trigo, R. M.: Hot and cold marine extreme events in the Mediterranean over the period 1982-  
992 2021, *Frontiers in Marine Science*, 9(August), 1–12,  
993 <https://doi.org/10.3389/fmars.2022.892201>, 2022.
- 994 Southward, A. J.: On changes of sea temperature in the english channel, *Journal of the*  
995 *Marine Biological Association of the United Kingdom*, 39(3), 449–458,  
996 <https://doi.org/10.1017/S0025315400013473>, 1960.
- 997 Wang, Y., Kajtar, J. B., Alexander, L. V., Pilo, G. S., and Holbrook, N. J.: Understanding the  
998 changing nature of marine cold-spells, *Geophysical Research Letters*, 49, e2021GL097002,  
999 <https://doi.org/10.1029/2021GL097002>, 2022.
- 1000 Wethey, D. S., and Woodin, S. A.: Climate change and *Arenicola marina*: Heat waves and the  
1001 southern limit of an ecosystem engineer, *Estuarine, Coastal and Shelf Science*, 276(December  
1002 2021), 108015, <https://doi.org/10.1016/j.ecss.2022.108015>, 2022.
- 1003 Wernberg, T., Bennett, S., Babcock, R. C., De Bettignies, T., Cure, K., Depczynski, M.,  
1004 Dufois, F., Fromont, J., Fulton, C. J., Hovey, R. K., Harvey, E. S., Holmes, T. H., Kendrick,  
1005 G. A., Radford, B., Santana-Garcon, J., Saunders, B. J., Smale, D. A., Thomsen, M. S.,  
1006 Tuckett, C. A., Tuya, F., Vanderklift, M. A., and Wilson, S.: Climate-driven regime shift of a  
1007 temperate marine ecosystem, *Science*, 353(6295), 169–172,  
1008 <https://doi.org/10.1126/science.aad8745>, 2016.
- 1009
- 1010 Vogel, M. M., Zscheischler, J., Wartenburger, R., Dee, D., and Seneviratne, S. I.: Concurrent  
1011 2018 hot extremes across Northern Hemisphere due to human-induced climate change.  
1012 *Earth's future*, 7(7), 692–703, <https://doi.org/10.1029/2019EF001189>, 2019.
- 1013

1014 Yao, Y., Wang, C., and Fu, Y.: Global Marine Heatwaves and Cold-Spells in Present Climate  
1015 to Future Projections, *Earth's Future*, 10(11), e2022EF002787, 2022.

1016

1017 Yiou, P., Cattiaux, J., Faranda, D., Kadygrov, N., Jézéquel, A., Naveau, P., Ribes, A., Robin,  
1018 Y., Thao, S., Oldenborgh, G. J. and Vrac, M.: Analyses of the Northern European summer  
1019 heatwave of 2018, *Bulletin of the American Meteorological Society*, 101(1), S35-S40,  
1020 <https://doi.org/10.1175/BAMS-D-19-0170.1ff>, 2020.

1021